



TÉCNICO LISBOA

Nonlinear Marine Animals Tracking System from Multiple USBL/INS Units

Nuno Miguel Vieira Pinto de Carvalho

Dissertação para a obtenção do grau de Mestre em

Engenharia Aeroespacial

Júri

Presidente: Prof. Doutor João Manuel Lage de Miranda Lemos
Orientador: Prof. Doutor Pedro Tiago Martins Batista
Co-orientador: Prof. Doutor Paulo Jorge Coelho Ramalho Oliveira
Vogal:
Vogal:

Outubro de 2013

Acknowledgments

I would like to start by thanking Professor Paulo Oliveira for allowing me the opportunity to integrate this project and motivating me through these few month of work. I would also like to thank Professor Pedro Batista for the availability and help in overcoming the difficulties I encountered.

I would also like to thank Eng. Bruno Carneira for his guidance during the lab work, and my colleagues Joel Reis, Marta Ribeiro, and Pedro Pereira.

Finally, a heartfelt thank to my friends, family, and my significant other for all the support and love they have given me in this journey.

This work was supported by project FCT PEst-OE/EEI/LA0009/2013 and by project FCT MAST/AM - PTFC/EEA - CRO/111107/2009.

Resumo

Nesta dissertação é apresentada uma nova técnica de fusão sensorial para seguimento de alvos subaquáticos, com aplicação ao estudo de animais marinhos, através de múltiplos *arrays* Ultra Short Baseline (USBL). A estratégia proposta baseia-se na utilização de alvos previamente marcados e utiliza informação de Direcção de Chegada de sinais acústicos provenientes do alvo obtida através dos *arrays*, a partir da diversidade espacial dos seus elementos. Dois métodos de obtenção da posição do alvo são desenvolvidos partindo da informação espacial disponível. Técnicas de estimação de Mínimos Quadrados e filtragem de *Kalman* são aplicadas ao problema e são desenhados algoritmos de Mínimos Quadrados Recursivos, Filtro de *Kalman* e EKF para aumentar a precisão das estimativas de posição e adicionar estimação de velocidade e aceleração do alvo. O desempenho das soluções desenvolvidas é avaliado e comparado com base em simulações numéricas.

Palavras-chave: seguimento de animais marinhos, USBL, estimação não-linear

Abstract

This thesis presents a new sensor fusion technique for tracking of underwater targets, with application to marine animal study, from multiple Ultra Short Baseline (USBL) receiver arrays. The proposed strategy is based on a marked target and relies on acoustic signal Direction of Arrival (DoA) information provided by the arrays and array relative positioning information. Two methods of obtaining the target position are devised based on the available spatial information. Least Squares (LS) and Kalman estimation techniques are applied in filtering approaches designed according to Recursive Least Squares (RLS), Kalman, and Extended Kalman Filter (EKF) methods, which yield increase position estimate accuracy and add velocity and acceleration estimation. The performance of the obtained solutions is evaluated and compared using simulation.

Keywords: marine animal tracking, USBL, nonlinear estimation

Contents

Acknowledgments	i
Resumo	iii
Abstract	v
Contents	viii
List of Figures	ix
List of Tables	xi
List of Symbols	xiv
Acronyms	xv
1 Introduction	1
1.1 Motivation	1
1.2 State of the Art	2
1.3 Problem Statement	4
1.4 Document Structure	5
2 Geometric Solution	7
2.1 Law of Sines Approach	7
2.2 Law of Cosines Approach	8
2.3 Validity Analysis	10
2.4 Simulation Setup	11
2.5 Simulation Results	13

3	Least Squares Estimation	19
3.1	Model Presentation	19
3.2	Loosely Coupled Implementation	22
3.3	Simulation Results	23
4	Kalman Filtering	29
4.1	Model Dynamics	29
4.2	Kalman Filtering Theory	31
4.3	Loosely Coupled Solution	33
4.4	Tightly Coupled Solution	34
4.5	Simulation Results	37
5	Conclusion and Future Work	49
6	Bibliography	51

List of Figures

- 1.1 VEMCO[®] example products 3
- 1.2 USBL array examples 4
- 1.3 Graphical representation of the mission scenario [12] 4

- 2.1 Graphical presentation of the problem situation 8
- 2.2 Graphical reinterpretation of the problem 9
- 2.3 Invalid Arrangements for the Law of Sines solution 11
- 2.4 Nominal trajectories for the considered simulations 12
- 2.5 Position estimate errors of the Law of Sines solution 15
- 2.6 Position estimate errors of the Law of Cosines solution 16
- 2.7 Position estimate errors of the Geometric solutions for the constant velocity case 17
- 2.8 Position estimate errors of the Geometric solutions for the constant acceleration case 17
- 2.9 Position estimate errors of the Geometric solutions for the sinusoidal velocity case 18

- 3.1 Position estimate errors of the RLS-V solution 24
- 3.2 Position estimate errors of the RLS-A solution 26
- 3.3 Position estimate errors of the RLS estimators for the constant velocity case 27
- 3.4 Position estimate errors of the RLS estimators for the constant acceleration case 27
- 3.5 Position estimate errors of the RLS estimators for the sinusoidal velocity case 28

- 4.1 Position estimate errors of the Kalman-V solution 41
- 4.2 Position estimate errors of the Kalman-A solution 42

4.3	Position estimate errors of the Kalman filters for the constant velocity case	43
4.4	Position estimate errors of the Kalman filters for the constant acceleration case	43
4.5	Position estimate errors of the Kalman filters for the sinusoidal velocity case	44
4.6	Position estimate errors of the EKF-V solution	45
4.7	Position estimate errors of the EKF-A solution	46
4.8	Position estimate errors of the Extended Kalman filters for the constant velocity case	47
4.9	Position estimate errors of the Extended Kalman filters for the constant acceleration case	47
4.10	Position estimate errors of the Extended Kalman filters for the sinusoidal velocity case	48

List of Tables

2.1	Measurements standard deviation	12
2.2	Estimate error mean and standard deviations for the Law of Sines solution	13
2.3	Estimate error mean and standard deviations for the Law of Cosines solution	13
2.4	Estimate RMS error comparisons for the geometric solutions	14
3.1	Estimate error mean and standard deviations for RLS-V solution	25
3.2	Estimate error mean and standard deviations for RLS-A solution	25
3.3	Estimate RMS error comparisons for the RLS solutions	26
4.1	Estimate error mean and standard deviations for Kalman-V solution	38
4.2	Estimate error mean and standard deviations for Kalman-A solution	38
4.3	Estimate RMS error comparisons for the Kalman filter solutions	39
4.4	Estimate error mean and standard deviations for EKF-V solution	40
4.5	Estimate error mean and standard deviations for EKF-A solution	40
4.6	Estimate RMS error comparisons for the EKF solutions	41

List of Symbols

α	angle between \mathbf{p}_t and \mathbf{p}_b
\mathbf{a}_{t_0}	initial target acceleration in the body-frame
β	angle between $-\mathbf{p}_b$ and \mathbf{p}_{tb}
$\Delta\tau$	difference in signal travel time between the target-vehicle and target-transponder paths
\mathbf{d}_{p_b}	transponder position direction cosine
\mathbf{d}_{p_t}	target position direction cosine
$\mathbf{d}_{p_{tb}}$	target position relative to the transponder direction cosine
γ	angle between \mathbf{p}_{tb} and \mathbf{p}_t
\mathbf{H}	discrete-time observation model matrix
\mathbf{p}_b	transponder position in the body-frame
\mathbf{p}_t	target position in the body-frame
\mathbf{p}_{tb}	target position relative to the transponder in the body-frame
\mathbf{p}_{t_0}	initial target position in the body-frame
τ	signal travel time between the target and the vehicle
τ_0	signal travel time between the transponder and the vehicle
\mathbf{v}_t	target velocity in the body-frame
\mathbf{v}_{t_0}	initial target velocity in the body-frame
t_{rt}	Round Trip Time
v_s	signal velocity
ξ	measurement error
\mathbf{A}	continuous-time dynamics model matrix

C	continuous-time observation model matrix
F_k	state transition matrix
K	Kalman gain matrix
P	estimation-error covariance matrix
R	measurement-error covariance matrix
x	state vector
y	measurement vector
ϵ_k	measurement residual
θ	estimation error

Acronyms

AWGN Additive White Gaussian Noise.

DoA Direction of Arrival.

EKF Extended Kalman Filter.

EKF-A Acceleration estimating EKF.

EKF-V Velocity estimating EKF.

Kalman-A Acceleration Estimating Kalman Filter.

Kalman-V Velocity Estimating Kalman Filter.

LBL Long Baseline.

LS Least Squares.

RLS Recursive Least Squares.

RLS-A Constant Acceleration Recursive Least Squares.

RLS-V Constant Velocity Recursive Least Squares.

RMS Root Mean Square.

SBL Short Baseline.

ToA Time of Arrival.

USBL Ultra Short Baseline.

Chapter 1

Introduction

1.1 Motivation

The importance of water in the existence of life has been one of the main driving forces of evolutionary processes, and its predominance across the Earth's surface has shaped human progress since the beginning of history. Some of the most important human settlements have been located in the vicinity of large bodies of water, be it rivers, lakes or oceans. Beyond the essential function of sustaining life, these bodies of water have found themselves deeply rooted in mankind's growth, progress, survival and culture for their great potential as sources of food and mineral wealth, their functions as ways of communication and transportation, their importance in energy generation and even for their leisure value.

Most recently, some of the gravest concerns regarding this seemingly immense environment are the depletion of marine food reserves due to overfishing and the effect of human activities in coastal waters in the health of marine flora and fauna. In order to study and understand the precise mechanisms that are at work in such situations, multidisciplinary teams of researchers involving marine biologists, scientists and engineers have been constituted into groups around the world. Additionally, this sort of study adds undeniable value in scientific knowledge from which expected and unexpected advances may arise as a result of observing the effects of pollution, fishing, transportation, oil drilling and many other activities on the health, behavior and migratory patterns of various marine species of interest.

Although a long running field of study, the tools used in this area of research have not developed much in recent years due to a number of issues including development and upgrade costs, backward compatibility considerations, maintenance concerns and others. The present work aims to explore advanced tracking techniques to be used in low cost tools with the intent of helping researchers by obtaining more accurate movement data on targeted individuals of marine animal populations.

1.2 State of the Art

Most current marine animal tracking systems in use worldwide work with electronic tags which can be broadly categorized as archival tags, transmission tags, or acoustic tags [11].

Archival tags work by collecting data such as time, water pressure, animal and water temperatures, and even satellite position. These are attached internally or externally to an animal and must be recovered in order to access the collected information. This may be accomplished through the recapture of the tagged animal or by pop-up mechanisms, which consists of the tag detaching itself from the tracked individual and floating to the surface.

Transmission tags gather similar information to archival tags. These, however, do not require recovery of the implanted hardware to recover the information gathered. By limiting the hardware to externally implanted tags, the data gathered can be remotely downloaded by researchers when the animals surface via satellite up-link or, if the tracked individual regularly visit coastal waters, via mobile communication networks.

The first two categories of tags incur in high deployment costs, the former due to the cost of having two missions, one for deployment and one for recovery, and the latter due to the higher complexity of the hardware and, especially in the case of the satellite up-link tags, the cost of the download bandwidth.

A less costly option are the acoustic category of tags. These can also be implanted internal or externally and transmit at semi-regular intervals acoustic pulses which may contain encoded identification, temperature and pressure data. The emitted pulses are then detected and decoded by a receiver if in range. The majority of acoustic tracking material is by, or compatible with, Canadian company VEMCO[©] receivers and transmitters.

Concerning the acoustic tags, these consist of pinger-type implantable devices of varying size that upon activation emit omni-directional semi-periodic acoustic pulses in which can be encoded information including identification, water pressure, and temperature data. Due to the level of complexity and specialization of these emitters, since there is already a wide market base using the systems, and that both emitter detection and its associated identification information decryption is available, these will be viewed as the standard and the work will be developed considering their limitations. An example of one such tag is represented in Fig. 1.1a.

As for the case of detectors, commercially available solutions are restricted to fixed or mobile presence detectors and manually operated directional detectors. The latter make use of directional hydrophones for which cost increases with precision. An example of the fixed receiver can be seen in Fig. 1.1b and an example of a mobile, manually operated receiver is in Fig. 1.1c respectively.



(a) V6 implantable tag [15]



(b) VR2 static receiver [16]



(c) VR100 portable receiver [16]

Figure 1.1: VEMCO[©] example products

A typical scenario of tracking animals with these systems requires implantation of the acoustic pinger in the intended target and the deployment of presence detectors in specified locations. These detectors use a single omni-directional hydrophone and can only mark the presence of the intended target in its effective range, logging it with any information carried by the signals. Mostly deployed in buoys, the information provided by such detectors is limited and implies several deployments with overlapping ranges in order to extract minimal and error prone trajectory information. This information has the added drawback of not being available in real-time, depending on data collection and cross-referencing.

In order to gather real-time precision information on animals directions relative to the receiver, directional hydrophones are used. However, due to the high costs, fragility, and the need for mechanical scanning in order to track a target, these are handled manually by researchers.

Parallely, position tracking systems have been studied for underwater applications and most used systems use arrays of omni-directional hydrophones or transducers in order to extract signal Direction of Arrival (DoA) from differences in Time of Arrival (ToA) between pairs of hydrophones using their spacial diversity. These arrays are usually divided into three major categories: Long Baseline (LBL), Short Baseline (SBL) and Ultra Short Baseline (USBL). The LBL arrays are fixed arrays that entail distances between transducers of hundreds of meters making these very expensive with a very complex calibration process and a high deployment time. The SBL arrays, are typically hull mounted arrays with distances in the tens of meters and that require constant monitoring of these distances due to the natural deforming of the structures that house the transducers. The USBL arrays are an evolution of the SBL systems with distances in the order of tens of centimeters that can be factory calibrated due to their smaller size and lesser deformation susceptibility. Furthermore, the latter, due to their reduced size, are flexible in mounting and deployment.

Although USBL systems are commercially available, for example the GAPS portable, pre-calibrated USBL in Fig. 1.2a, this work will be based on the assumption that an

in-house solution being developed in parallel, the MAST-AM tool seen in Fig. 1.2b, will be used. This allows for full control over the reception hardware and detection algorithms.



(a) GAPS portable, pre-calibrated USBL [5]



(b) MAST-AM tool

Figure 1.2: USBL array examples

1.3 Problem Statement

The object of this work consists in determining the position of a moving target in an underwater environment through the use of acoustic signals. The target is equipped with an acoustic pinger type marker which produces a signal in which an identification number may be encoded. In order to determine the position of this target, two receivers are available. A manned underwater tool used for aiding a diver in the identification, tracking and observation of the target, and a surface transponder, used for precise target positioning and diver localization in an inertial frame. Both the tool and the transponder are equipped with hydrophone arrays in an inverted-USBL configuration, which are used to obtain a DoA from a received signal. The assumed mission scenario is depicted in Fig. 1.3.

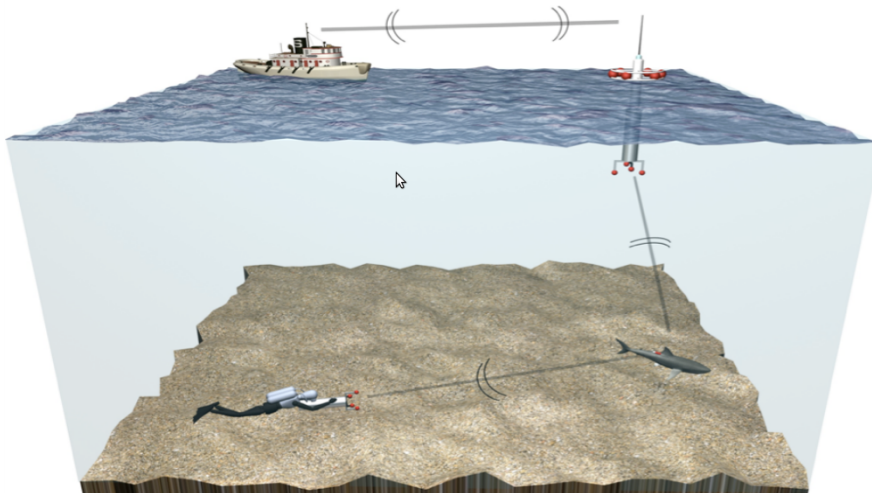


Figure 1.3: Graphical representation of the mission scenario [12]

Based on the work in [8], it is possible for a vehicle equipped with an USBL array

to obtain its relative position to a similarly equipped transponder which is assumed as stationary in the inertial frame. This is accomplished through the transmission of an acoustic signal by the first which is detected by the USBL array present on the latter, and the emission of a response by the transponder and corresponding reception by the vehicle-mounted array. Such an operation allows each receptor to determine its counterpart's direction in their respective body-frames, resorting to the plane-wave approximations to the received signal and from the differences in ToA between pairs of elements in the hydrophone arrays, obtain the DoA of said signal and relative direction of its source.

Furthermore, the distance between both objects can be determined by the emission of an interrogating signal from one and an adequate response from the other. By measuring the time between the interrogation and the reception of the response it is possible to obtain the round-trip time (t_{rt}), assuming that the response involves a fixed and known delay between the reception of the interrogations and the emission of the response. With the already available DoA of the response signal available, this measurement of time allows for the full precise positioning of the transponder in the vehicle's body-frame, and vice versa, assuming a constant known speed of sound in the medium.

At this point, the focus of this work is the third element, the moving target. Since the target is tagged with a pinger type marker, the range cannot be measured in the same way as the vehicle-transponder range. Thus an indirect form of range measurement must be used and its development is the subject of Chapter 2.

1.4 Document Structure

In this document a number of advanced tracking techniques are developed for underwater acoustic tracking of marine animals. In Chapter 2 it is shown how, with the available information, the initial part of the problem, the target position, may be determined using two similar algebraic geometrical approaches, and also their limitations. The performance of the devised solutions is then evaluated in the presence of noisy measurements by defining a set of simulation parameters, to be used in the evaluation of all future solutions, and using them to observe the error of the proposed methods. In Chapter 3, Least Squares (LS) parameter estimation techniques are applied to the problem, a loosely coupled Recursive Least Squares (RLS) estimator is designed using position data calculated externally using the previously designed algebraic solutions, and afterwards is simulated in the previously specified conditions and the results evaluated. In Chapter 4, the Kalman Filtering technique is used to improve on the RLS estimator, in loosely and tightly coupled implementations, the latter removing the need for external computations. Firstly, the loosely coupled solution is implemented in a linear Kalman filter, in a structure similar to the previously designed linear RLS estimator, and afterwards the non-linear tightly coupled solution is implemented in an Extended Kalman Filter (EKF).

Chapter 2

Geometric Solution

2.1 Law of Sines Approach

In Fig. 2.1, the mission scenario is depicted with the available positioning elements and measurements. In this problem all quantities are indicated as represented in the body-frame of the vehicle and as such, the vehicle's position is always the origin of the frame. From this we define the target position vector \mathbf{p}_t and the transponder position vector \mathbf{p}_b as the vectors that give the respective positions in the frame of reference. Additionally, we define \mathbf{p}_{tb} as the vector that, in the vehicle's body-frame, represents the position of the target relative to the position of the transponder. For these vectors, their direction cosines are defined as \mathbf{d}_{pt} , \mathbf{d}_{pb} , and \mathbf{d}_{ptb} respectively for \mathbf{p}_t , \mathbf{p}_b , and \mathbf{p}_{tb} .

It is possible from the figure to identify a simple triangular geometry for the problem. Firstly, this triangle is in a three dimensional space and any three non collinear points form a plane in such a frame. Thus, assuming the situation of non collinearity of the three elements of the problem holds, then their three positions in the body frame of the vehicle can be used as the plane defining points. With this in mind, we can observe that any measurements taken between any two elements of the problem are from two points in a same plane and thus these measurements are projected in that plane. Therefore, the three dimensional problem in the three dimensional space may be represented, without loss of information, as a problem in a plane within the three dimensional space and may be solved accordingly.

Based on the considerations above, the problem can be viewed as solving a triangle of which some elements are directly measurable by the vehicle, namely the direction cosines \mathbf{d}_{pt} , \mathbf{d}_{pb} , and the vehicle-transponder distance $\|\mathbf{p}_b\|$. Additionally, the director cosine \mathbf{d}_{ptb} is directly measurable by the transponder and may be made available to the vehicle. At this point, there are enough elements to allow for the complete and unambiguous determination of the target distance and, consequently, its position in the vehicle's body-frame.

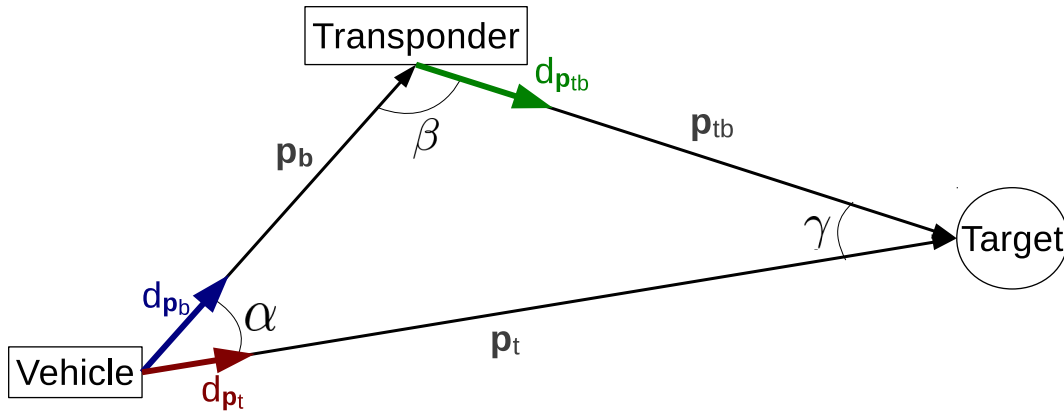


Figure 2.1: Graphical presentation of the problem situation

According to the figure, let

$$\cos \alpha = \mathbf{d}_{p_t} \cdot \mathbf{d}_{p_b} \quad (2.1)$$

and

$$\cos \beta = \mathbf{d}_{p_{tb}} \cdot (-\mathbf{d}_{p_b}) , \quad (2.2)$$

And, according to the internal angles of a triangle, let also

$$\gamma = \pi - \alpha - \beta . \quad (2.3)$$

There are now enough available elements of the triangle geometry to allow the determination of its remaining elements using the Law of Sines

$$\frac{\|\mathbf{p}_t\|}{\sin \beta} = \frac{\|\mathbf{p}_b\|}{\sin \gamma} , \quad (2.4)$$

Which can be rearranged in order to isolate the target range as

$$\|\mathbf{p}_t\| = \frac{\sin \beta}{\sin \gamma} \|\mathbf{p}_b\| . \quad (2.5)$$

The determination of the complete target position is completed by multiplying the computed target range, $\|\mathbf{p}_t\|$, by the measured target position direction cosine, \mathbf{d}_{p_t} .

2.2 Law of Cosines Approach

An alternative to the Law of Sines approach may be devised, using relations between the distances $\|\mathbf{p}_t\|$ and $\|\mathbf{p}_{tb}\|$, based on the physical characteristics of the acoustic signal used to track the target.

Due to the nature of the problem, the emitted signal from the target is transmitted simultaneously to both the transponder and the vehicle from the target. Thus, each length traveled by the signal to each of the receivers can be expressed as a product of the signal

velocity, v_s , by a time, τ , which it takes to reach that receiver. Assuming a known and constant v_s throughout the length of travel and due to the fact that the signal is emitted at the same point in time for both \mathbf{p}_t and \mathbf{p}_{tb} paths, their difference in length can be expressed through a difference of travel time, $\Delta\tau$. This reinterpretation of the problem, presented in Fig. 2.2, has the reference travel time τ coupled to the $\|\mathbf{p}_{tb}\|$ interval, as before, the \mathbf{p}_b vector is available through direct measurements and τ_0 is the travel time between the vehicle and the transponder. At this point, the problem distances can be rewritten accordingly.

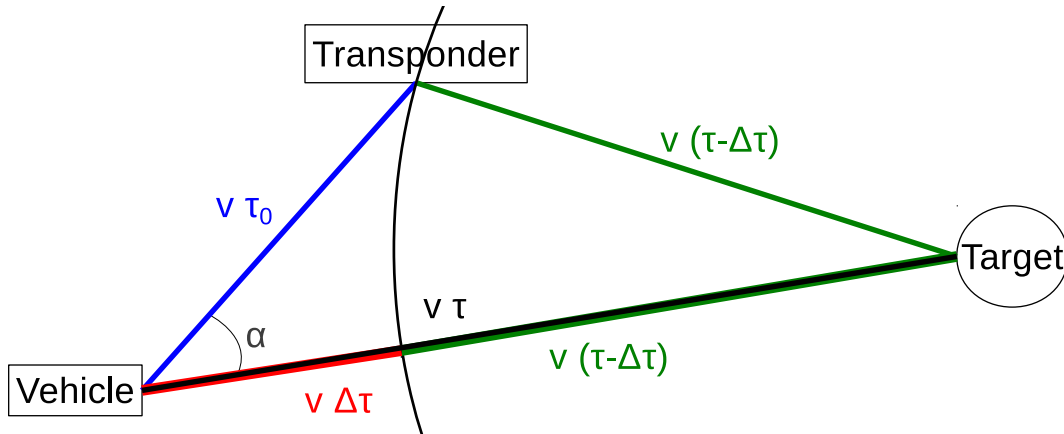


Figure 2.2: Graphical reinterpretation of the problem

Let the target range be given as

$$\|\mathbf{p}_t\| = v_s \tau , \quad (2.6)$$

the transponder range as

$$\|\mathbf{p}_b\| = v_s \tau_0 , \quad (2.7)$$

and the distance between the transponder and the target as

$$\|\mathbf{p}_{tb}\| = v_s (\tau - \Delta\tau) , \quad (2.8)$$

in which τ is the travel time from the target to the vehicle, τ_0 is the travel time between the vehicle and the transponder and $\Delta\tau$ is the difference in signal travel time between the emitter-vehicle and the emitter-transponder paths.

By applying the distributive property to (2.8) and substituting (2.6) into it gives, after rearranging,

$$\Delta\tau = \frac{\|\mathbf{p}_t\| - \|\mathbf{p}_{tb}\|}{v_s} . \quad (2.9)$$

Using this redefinition of the problem variables it is possible to use a Law of Cosines approach to relate the new quantities. Applying the Law of Cosines to the triangle in Fig. 2.2 gives

$$\|\mathbf{p}_{tb}\|^2 = \|\mathbf{p}_t\|^2 + \|\mathbf{p}_b\|^2 - 2\|\mathbf{p}_t\|\|\mathbf{p}_b\| \cos \alpha \quad (2.10)$$

and replacing (2.6), (2.7), and (2.8) in (2.10) finds

$$[v_s (\tau - \Delta\tau)]^2 = (v_s \tau)^2 + (v_s \tau_0)^2 - 2(v_s \tau)(v_s \tau_0) \cos \alpha . \quad (2.11)$$

Both sides of equation (2.11) can be divided by v_s^2 resulting in

$$(\tau - \Delta\tau)^2 = \tau^2 + \tau_0^2 - 2 \tau \tau_0 \cos \alpha , \quad (2.12)$$

which rewritten for τ gives

$$\tau = \frac{\tau_0^2 - \Delta\tau^2}{2(\tau_0 \cos \alpha - \Delta\tau)} . \quad (2.13)$$

By transmission of a target detected signal from the transponder to the vehicle, the time difference $\Delta\tau$ can be directly obtained if a constant and known delay is added by the transponder, by subtracting from the time difference between the reception of the target signal and the transponder target detection signal, the transponder-vehicle travel time and the known transponder delay. With this information, the target distance signal travel time, τ , can be computed.

With this determination of τ , inserting it in (2.6), gives the calculated target range. In order to determine a position from this value it is a matter of multiplying this scalar value with the direction cosine \mathbf{d}_{p_t} , already available through direct measurement.

2.3 Validity Analysis

After devising two methods of finding the target position, it is of interest to study in which situations these methods degrade their computations and become unusable. Firstly let us remember the Law of Sines approach (2.5)

$$\|\mathbf{p}_t\| = \frac{\sin \beta}{\sin \gamma} \|\mathbf{p}_b\| .$$

This equation can not be applied when the denominator approaches zero, resulting in

$$\sin \gamma = 0 \Leftrightarrow \gamma = k\pi, k \in \mathbb{Z} \quad (2.14)$$

which, for the considered situation geometrical constraints, may take only two physically acceptable values

$$\gamma = 0 \vee \gamma = \pi \quad (2.15)$$

Translating these values into the problem geometry, it means that the proposed method breaks down precisely as it approaches the limits of the assumption validity, namely the non-collinearity hypothesis. These considerations are represented in Fig. 2.3. Additionally, there is one further situation in which the method fails, which is for a triangle in which the $\|\mathbf{p}_t\|$ dimension is much larger than $\|\mathbf{p}_b\|$ and forces γ to approach zero.

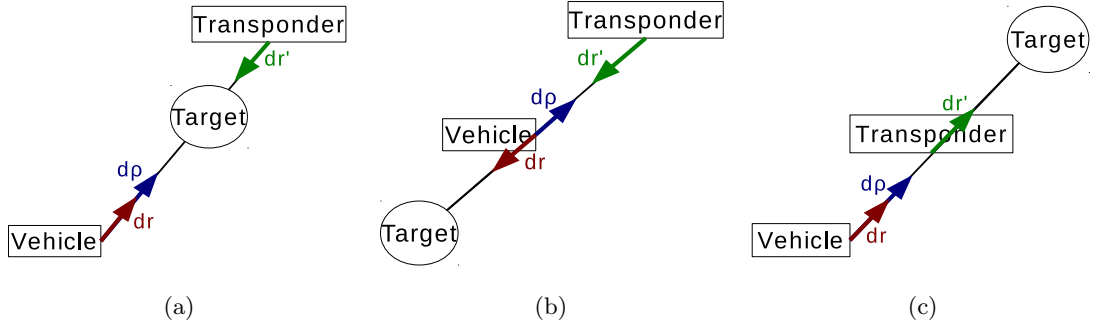


Figure 2.3: Invalid Arrangements for the Law of Sines solution

Let us now observe the expression for the delay obtained with (2.13) of the Law of Cosines approach

$$\tau = \frac{\tau_0^2 - \Delta\tau^2}{2(\Delta\tau + \tau_0 \cos \alpha)} .$$

This solution is invalid if at any time the denominator of the equation becomes zero

$$\begin{aligned} 2(\tau_0 \cos \alpha - \Delta\tau) &= 0 \\ \tau_0 \cos \alpha &= \Delta\tau . \end{aligned} \quad (2.16)$$

Multiplying both sides of (2.16) by v_s and substituting (2.7) and (2.9) results in

$$\|\mathbf{p}_b\| \cos \alpha = \|\mathbf{p}_t\| - \|\mathbf{p}_{tb}\| . \quad (2.17)$$

By rearranging (2.10) into

$$\cos \alpha = \frac{\|\mathbf{p}_{tb}\|^2 - \|\mathbf{p}_t\|^2 - \|\mathbf{p}_b\|^2}{-2\|\mathbf{p}_t\|\|\mathbf{p}_b\|} \quad (2.18)$$

and substituting into (2.17) gives

$$\begin{aligned} \|\mathbf{p}_b\| \frac{\|\mathbf{p}_{tb}\|^2 - \|\mathbf{p}_t\|^2 - \|\mathbf{p}_b\|^2}{-2\|\mathbf{p}_t\|\|\mathbf{p}_b\|} &= \|\mathbf{p}_t\| - \|\mathbf{p}_{tb}\| \\ \|\mathbf{p}_b\|^2 &= \|\mathbf{p}_t\|^2 - 2\|\mathbf{p}_t\|\|\mathbf{p}_{tb}\| + \|\mathbf{p}_{tb}\|^2 \\ \|\mathbf{p}_b\| &= \|\mathbf{p}_t\| - \|\mathbf{p}_{tb}\| . \end{aligned} \quad (2.19)$$

The final result of (2.19) represents, for a triangle, the situation represented in Fig. 2.3c.

2.4 Simulation Setup

In order to validate the developed solutions, numerical simulations were carried out covering a range of model behaviors assumed to be valid for the targets. In all situations, the measurements are assumed to be corrupted with zero-mean Additive White Gaussian Noise (AWGN) with standard deviations given in Table 2.1.

Measurement	AWGN Standard deviation
α angle	0,5 [deg]
β angle	0,5 [deg]
$\ \mathbf{d}_{p_b}\ $	1 [m]
$\Delta\tau$	100 [μs]

Table 2.1: Measurements standard deviation

Three trajectories are considered for this purpose. The first is a constant velocity situation, as presented in Fig. 2.4a, the second is a constant acceleration case, represented in Fig. 2.4b, and finally a sinusoidal velocity situation, shown in Fig. 2.4c. All of the situations are modeled for a mission time of 150 seconds with a time step of 1 second.

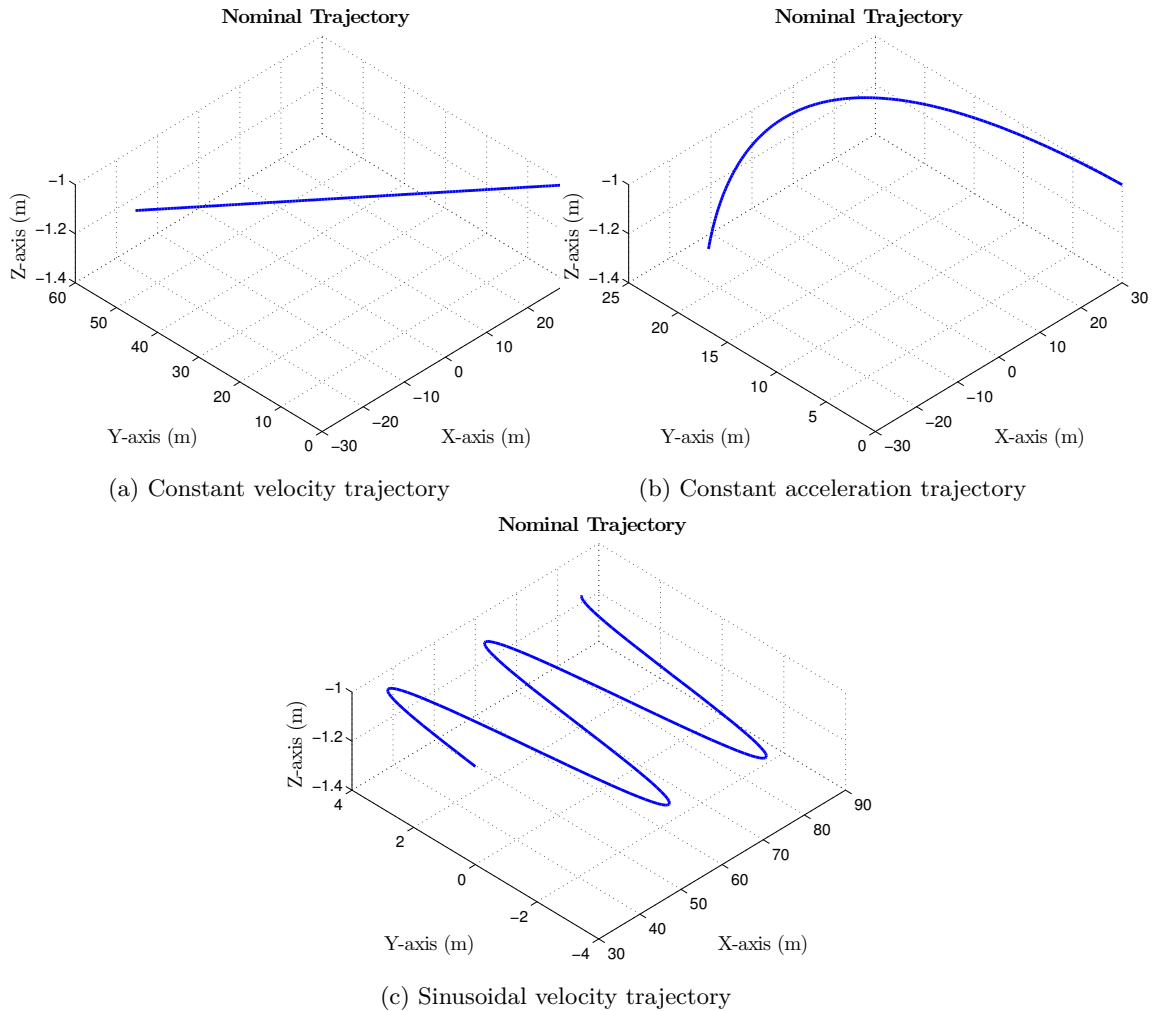


Figure 2.4: Nominal trajectories for the considered simulations

In all cases, the transponder is fixed at $\mathbf{p}_b = \begin{bmatrix} 15 & 10 & 2 \end{bmatrix} m$ and the target starts at $\mathbf{p}_t = \begin{bmatrix} 30 & 0 & -1 \end{bmatrix} m$. For the first situation the velocity is fixed at $\mathbf{v}_1 = \begin{bmatrix} -1 & 1 & -0.002 \end{bmatrix} ms^{-1}$, for the second case the velocity begins at $\mathbf{v}_2 = \begin{bmatrix} 0 & 1 & -0.002 \end{bmatrix} ms^{-1}$ and the acceler-

ation is fixed at $\mathbf{a} = \begin{bmatrix} -0.005 & -0.005 & 0 \end{bmatrix} m s^{-2}$, and for the third case the velocity starts as $\mathbf{v}_3 = \mathbf{v}_1$ and its v_{3y} component varies with $v_{3y} = \cos 2\pi ft m s^{-1}$ with a frequency $f = 0.015 Hz$. The speed of sound (v_s) in the medium is also assumed known and constant, $v_s = 1560 m s^{-1}$.

2.5 Simulation Results

In order to validate the solutions obtained and expressed respectively by (2.5) and (2.13), these were implemented in simulations described in section 2.4. Predictably, the use of the equations in the absence of noise resulted in a perfect reproduction of the real values of range and position. The addition of noise produced expected errors in the calculated target positions. Furthermore a difference in performance was noticeable between both methods. Firstly the position estimate errors are shown in Fig. 2.5 and 2.6 and their results are described in Table 2.2 and 2.3.

	$p_x (m)$		$p_y (m)$		$p_z (m)$	
	μ	σ	μ	σ	μ	σ
Constant Velocity	0.1141	1.0850	-0.0834	1.7404	-0.0203	0.2740
Constant Acceleration	-0.1764	1.3686	0.0020	1.0907	-0.0170	0.2702
Sinusoidal Velocity	0.7361	5.2655	-0.0548	0.5255	0.0033	0.6267

Table 2.2: Estimate error mean and standard deviations for the Law of Sines solution

	$p_x (m)$		$p_y (m)$		$p_z (m)$	
	μ	σ	μ	σ	μ	σ
Constant Velocity	-0.0623	0.9926	0.1324	1.8459	-0.0246	0.2831
Constant Acceleration	-0.2393	1.3401	-0.0677	1.0121	-0.0161	0.2766
Sinusoidal Velocity	1.5788	8.5595	-0.0637	0.5408	-0.0142	0.6440

Table 2.3: Estimate error mean and standard deviations for the Law of Cosines solution

The results shown in Fig. 2.5 and 2.6, and characterized in Tables 2.2 and 2.3 allow for some conclusions on the performance of geometric solutions. However, they do not necessarily impart the full influence on the total position estimate. For this, the norm of the vector difference between the estimate and the real target position was computed at each step representing the total prediction error. The results are shown in Fig. 2.7, 2.8, and 2.9.

Starting with Fig. 2.7, it is possible to observe that, overall, both methods have similar behavior in the considered trajectory, differing in error levels at different stages in the trajectory, while maintaining a target position error mostly below 12% of the true range.

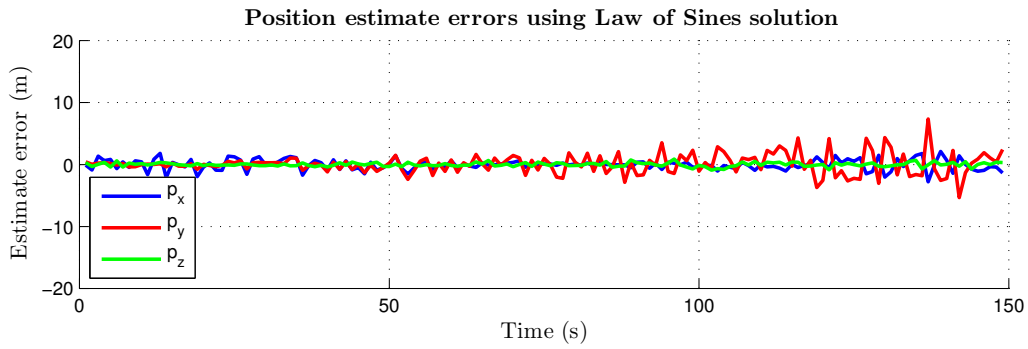
From Fig. 2.8, an area of significant divergence between both methods estimates is noticeable, with a sharp rise in the estimated position error of the Law of Cosines approach, around the time instant 50 s of the simulation.

Finally, from Fig. 2.9 the estimate errors of both solutions initially presents a similar behavior, in accordance to the observations of the previous simulation results. However, at approximately the 75 second instant in the simulation, the errors grow rapidly. This may be attributed to the increase in the true range of the target. As has been seen in section 2.3, the position estimate given by the Law of Sines approach deteriorates with the increase in range and since the true range of the considered simulation continuously increases with time, this behavior is expected.

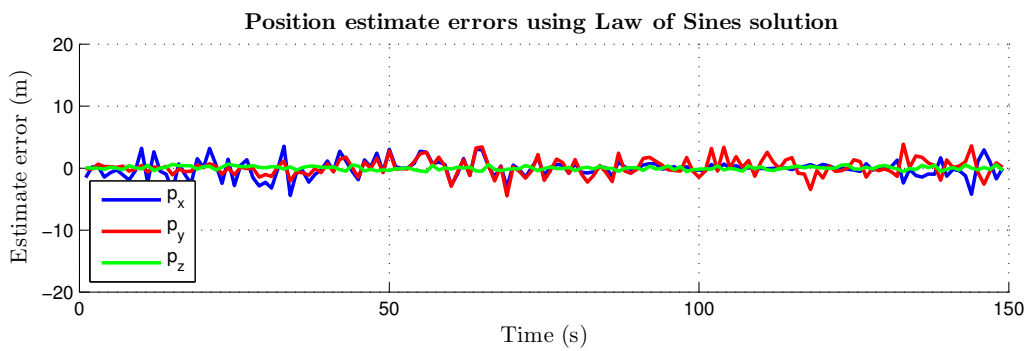
In order to evaluate the best solution to use in further developments, the Root Mean Square (RMS) of the estimate error norm is computed for the final 50 seconds of simulation and is presented in Table 2.4, from which can be determined that the most accurate approach is the Law of Sines solution and it will thus be the chosen method for all future developments.

Simulation	Law of Sines	Law of Cosines
Constant Velocity	3.0873 (m)	3.8765 (m)
Constant Acceleration	1.6665 (m)	1.0405 (m)
Sinusoidal Velocity	7.8186 (m)	13.7981 (m)

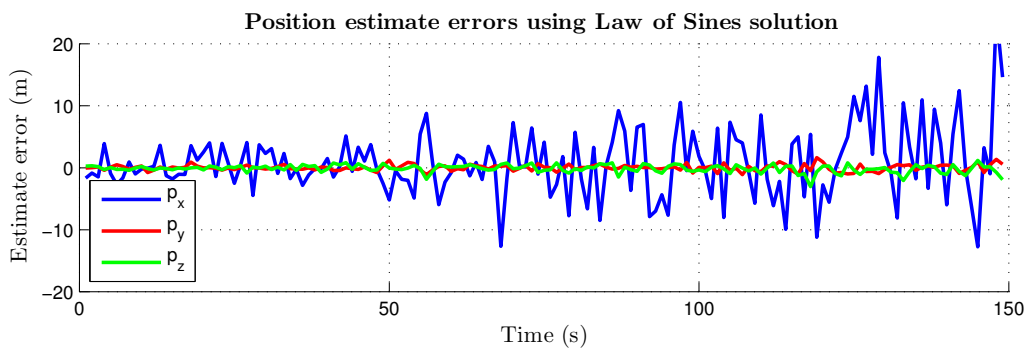
Table 2.4: Estimate RMS error comparisons for the geometric solutions



(a) Constant Velocity trajectory

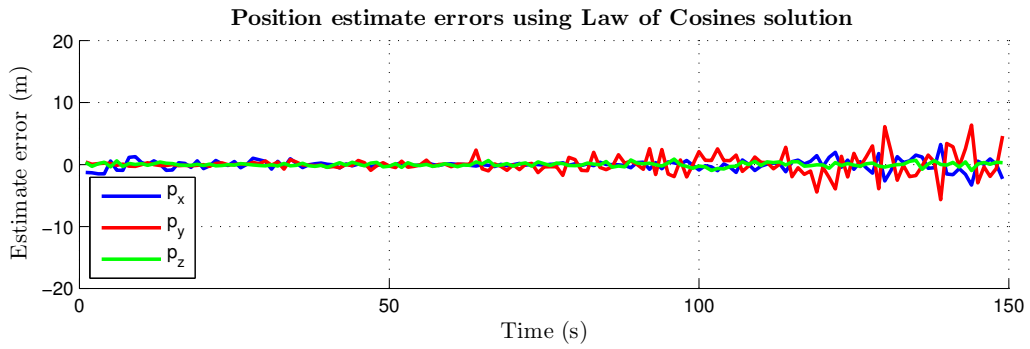


(b) Constant Acceleration trajectory

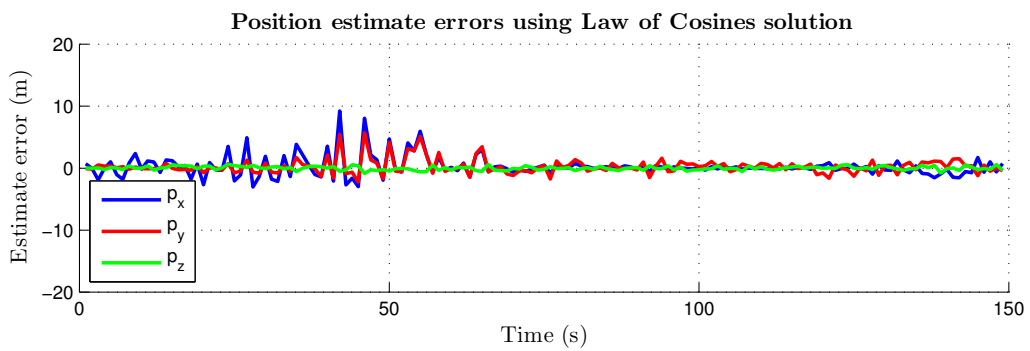


(c) Sinusoidal Velocity trajectory

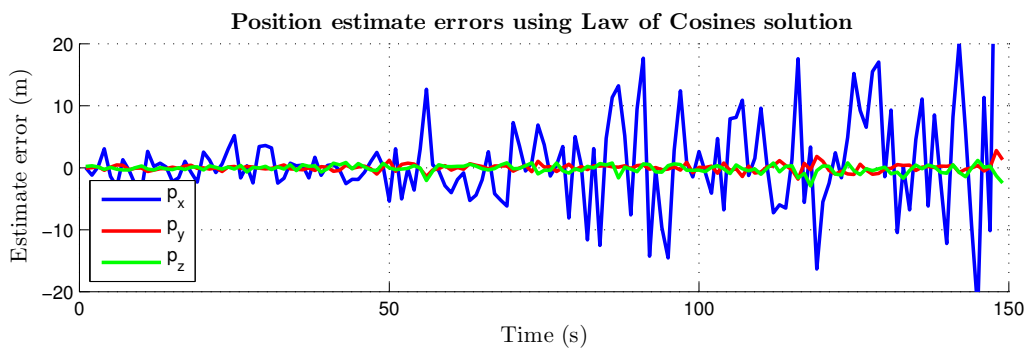
Figure 2.5: Position estimate errors of the Law of Sines solution



(a) Constant Velocity trajectory



(b) Constant Acceleration trajectory



(c) Sinusoidal Velocity trajectory

Figure 2.6: Position estimate errors of the Law of Cosines solution

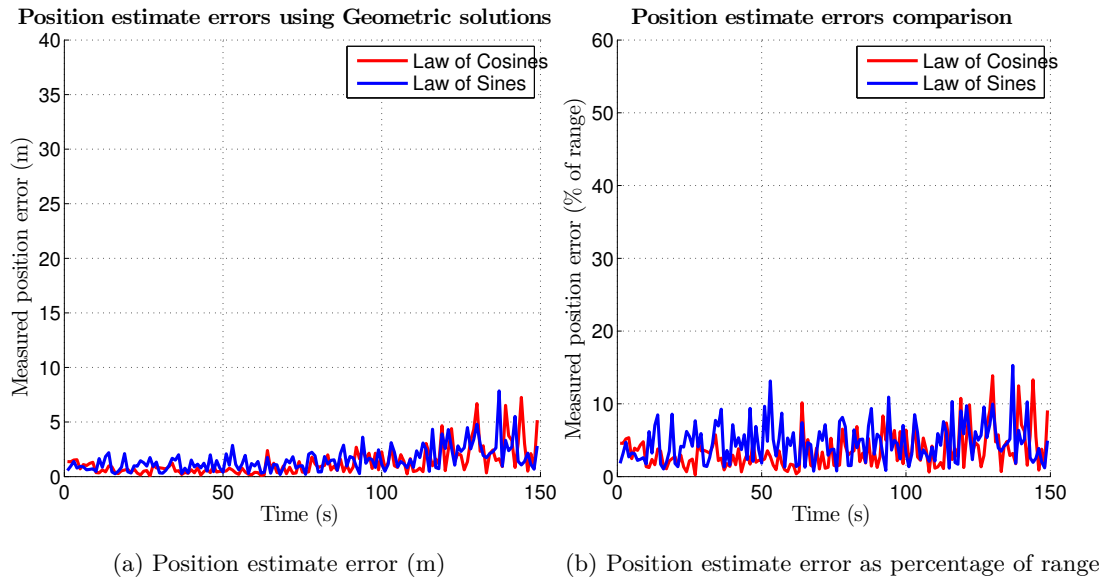


Figure 2.7: Position estimate errors of the Geometric solutions for the constant velocity case

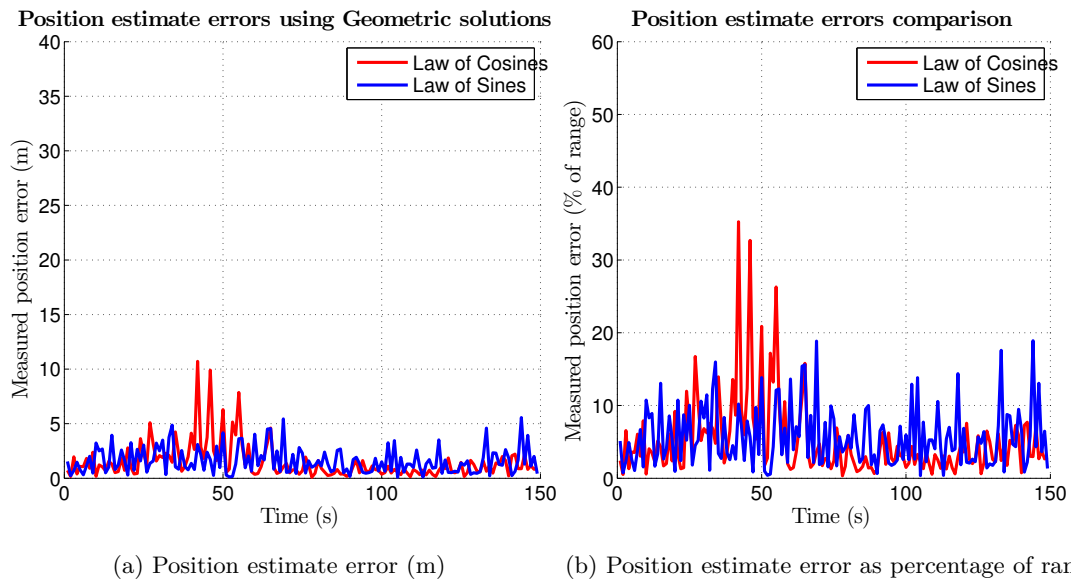


Figure 2.8: Position estimate errors of the Geometric solutions for the constant acceleration case

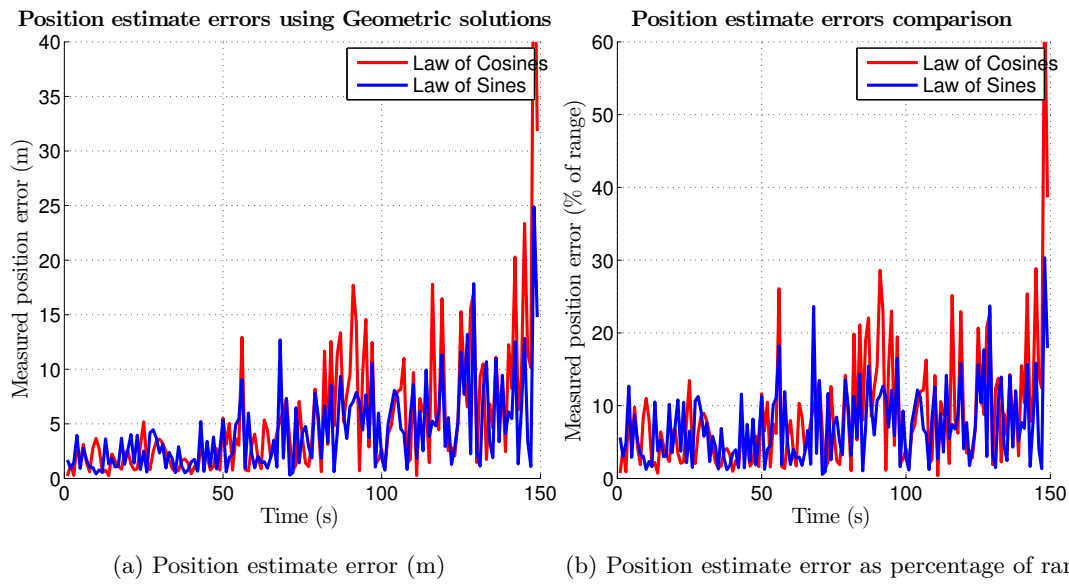


Figure 2.9: Position estimate errors of the Geometric solutions for the sinusoidal velocity case

Chapter 3

Least Squares Estimation

3.1 Model Presentation

From the previous section, the position of a target has been found to be obtainable in the receiver's body-frame, with an error that is proportional to the real distance between the receivers and the target. This provides inaccurate results, thus the need for a solution that minimizes the error between the position estimates and the real positions of the target.

The first technique used for increasing the accuracy of the estimates is performed in a Least Squares (LS) estimator, chosen due to its computational and theoretical simplicity. This type of estimator requires a model based on unknown constant parameters, to which the measurements are fitted. In this work we will begin by assuming a Newtonian kinematic model of constant acceleration which has the characteristic position and velocity equations

$$\mathbf{p}_t(t) = \mathbf{p}_{t_0} + \mathbf{v}_{t_0}t + \frac{1}{2}\mathbf{a}_{t_0}t^2 \quad (3.1)$$

and

$$\mathbf{v}_t(t) = \mathbf{v}_{t_0} + \mathbf{a}_{t_0}t, \quad (3.2)$$

where $\mathbf{p}_t(t)$ and $\mathbf{v}_t(t)$ are the target position, and velocity at time t , respectively, and \mathbf{p}_{t_0} , \mathbf{v}_{t_0} and \mathbf{a}_{t_0} are constants representing the initial target position, velocity and acceleration, respectively.

With the chosen model, the position of the target at any time, is obtainable with knowledge of the three initial conditions of the motion (\mathbf{p}_{t_0} , \mathbf{v}_{t_0} and \mathbf{a}_{t_0}) and the present time by means of (3.1). Since it has been established that it is possible to obtain measurements of the target position in some instants of known t , this problem may be solved through the fitting of (3.1) to the data points measured in order to determine the problem constants.

For a least squares solution to be possible, any k^{th} element of a measurement vector \mathbf{y} , \mathbf{y}_k , must be a linear combination of the elements of a constant parameter vector \mathbf{x} to

be estimated with the addition of some measurement noise v . It may be expressed as

$$\mathbf{y}_k = \sum_{i=1}^n H_{ki} \mathbf{x}_i + v_k \quad (3.3)$$

or, in matrix form,

$$\mathbf{y}_k = \mathbf{H}_k \mathbf{x} + v_k . \quad (3.4)$$

Since the measurement vector is, by definition,

$$\mathbf{y} = \left[\mathbf{y}_1 \quad \cdots \quad \mathbf{y}_k \right]^T , \quad (3.5)$$

the entire measurement vector can be related to \mathbf{x} through

$$\mathbf{y} = \mathbf{H} \mathbf{x} + v , \quad (3.6)$$

with

$$\mathbf{H} = \begin{bmatrix} H_{11} & \cdots & H_{1n} \\ \vdots & \ddots & \vdots \\ H_{k1} & \cdots & H_{kn} \end{bmatrix} \quad (3.7)$$

and

$$\mathbf{x} = \left[x_1 \quad \cdots \quad x_n \right]^T . \quad (3.8)$$

As the objective of this method is to approximate a model, through the parameter vector, to a number of measurements, it may be viewed as minimizing an error between the model and the measurements and thus an element ϵ_k can be defined, called the measurement residual, as the difference between a measurement \mathbf{y}_k and the model's prediction for such measurement as

$$\epsilon_k = \mathbf{y}_k - \mathbf{H}_k \hat{\mathbf{x}} , \quad (3.9)$$

where $\hat{\mathbf{x}}$ is the estimate of the parameter vector. Since the best estimate of \mathbf{x} is given by the vector $\hat{\mathbf{x}}$ that minimizes the sum of the squares of the measurement residuals, the objective is to find the estimate that minimizes a cost function of the form

$$J = \sum_k \epsilon_k^2 = \boldsymbol{\epsilon}^T \boldsymbol{\epsilon} , \quad (3.10)$$

in which $\boldsymbol{\epsilon}$ is the measurement residual vector given as

$$\boldsymbol{\epsilon} = \left[\epsilon_1 \quad \cdots \quad \epsilon_k \right]^T = \mathbf{y} - \mathbf{H} \hat{\mathbf{x}} . \quad (3.11)$$

By substituting (3.11) into (3.10), we can express the cost function as

$$\begin{aligned} J &= \boldsymbol{\epsilon}^T \boldsymbol{\epsilon} = (\mathbf{y} - \mathbf{H} \hat{\mathbf{x}})^T (\mathbf{y} - \mathbf{H} \hat{\mathbf{x}}) \\ &= \mathbf{y}^T \mathbf{y} - \hat{\mathbf{x}}^T \mathbf{H}^T \mathbf{y} - \mathbf{y}^T \mathbf{H} \hat{\mathbf{x}} + \hat{\mathbf{x}}^T \mathbf{H}^T \mathbf{H} \hat{\mathbf{x}} , \end{aligned} \quad (3.12)$$

and to find its minimum, the partial derivative with respect to the estimate is computed and is set equal to zero

$$\frac{\partial J}{\partial \hat{\mathbf{x}}} = -\mathbf{y}^T \mathbf{H} - \mathbf{y}^T \mathbf{H} + 2 \hat{\mathbf{x}}^T \mathbf{H}^T \mathbf{H} = 0 , \quad (3.13)$$

$$\mathbf{H}^T \mathbf{y} = \mathbf{H}^T \mathbf{H} \hat{\mathbf{x}} , \quad (3.14)$$

and finally the best estimate of \mathbf{x} is then given by

$$\hat{\mathbf{x}} = (\mathbf{H}^T \mathbf{H})^{-1} \mathbf{H}^T \mathbf{y} . \quad (3.15)$$

However, using this approach requires that a record be maintained of every measurement taken in the \mathbf{y} vector as well as requiring an ever expanding \mathbf{H} matrix. This is computationally expensive and due to the unpredictable number of measurements is inadvisable. In order to circumvent this issue a recursive estimation method is of interest and thus the Recursive Least Squares (RLS) method is used. This approach provides the least squares estimate recursively with each new available measurement based on the previous estimate and an estimation-error covariance estimate. A different cost function is also chosen to be minimized. This new function, defined in (3.17) as the sum of the estimate-error variances at each time step, leads to the addition of a dependence on the variance of the noisy measurements through a measurement-error covariance matrix to be later defined.

Taking (3.4), a linear recursive estimator can be written in the form

$$\hat{\mathbf{x}}_k = \hat{\mathbf{x}}_{k-1} + \mathbf{K}_k (\mathbf{y}_k - \mathbf{H}_k \hat{\mathbf{x}}_{k-1}) , \quad (3.16)$$

where $\hat{\mathbf{x}}_{k-1}$ is the estimate after measurement \mathbf{y}_{k-1} and $\hat{\mathbf{x}}_k$ is the estimate after measurement \mathbf{y}_k . The \mathbf{K}_k matrix is the estimator gain and is obtained by minimizing the new cost function

$$J_k = \sum_i^n E [\theta_{ik} \theta_{ik}] \quad (3.17)$$

$$\frac{\partial J_k}{\partial \mathbf{K}_k} = \frac{\partial}{\partial \mathbf{K}_k} \left(E \left[\sum_i^n \theta_{ik} \theta_{ik} \right] \right) = 0 \quad (3.18)$$

in which θ_{nk} is the estimation error for the n^{th} parameter at the k^{th} step

$$\theta_{nk} = \mathbf{x}_{nk} - \hat{\mathbf{x}}_{nk} , \quad (3.19)$$

with

$$\boldsymbol{\theta}_k = \left[\theta_{1k} \quad \cdots \quad \theta_{nk} \right]^T . \quad (3.20)$$

By defining an estimation-error covariance matrix \mathbf{P}_k as an $n \times n$ diagonal matrix with

$$\mathbf{P}_k = E \left(\boldsymbol{\theta}_k \boldsymbol{\theta}_k^T \right) \quad (3.21a)$$

$$Tr \left(\mathbf{P}_k \right) = E \left(\boldsymbol{\theta}_k^T \boldsymbol{\theta}_k \right) , \quad (3.21b)$$

using (3.21) in (3.18), the latter can be simplified to

$$\frac{\partial J_k}{\partial \mathbf{K}_k} = 2 \left(\mathbf{I} - \mathbf{K}_k \mathbf{H}_k \right) \mathbf{P}_{k-1} \left(-\mathbf{H}_k^T \right) + 2 \mathbf{K}_k \mathbf{R}_k = 0 , \quad (3.22)$$

where \mathbf{P}_{k-1} is the estimation-error covariance matrix of the previous step and \mathbf{R}_k is the measurement-error covariance matrix. The latter presents similar expressions to (3.21), substituting the estimation error $\boldsymbol{\theta}$ with the measurement error $\boldsymbol{\xi}$

$$\mathbf{R}_k = E(\boldsymbol{\xi}_k \boldsymbol{\xi}_k^T) \quad (3.23a)$$

$$\boldsymbol{\xi}_k = \mathbf{y}_k - \hat{\mathbf{y}}_k. \quad (3.23b)$$

Solving (3.22) for the gain matrix gives

$$\mathbf{K}_k = \mathbf{P}_{k-1} \mathbf{H}_k^T (\mathbf{H}_k \mathbf{P}_{k-1} \mathbf{H}_k^T + \mathbf{R}_k)^{-1} \quad (3.24)$$

and the estimation-error covariance matrix for the present step is found from (3.21a)

$$\mathbf{P}_k = (\mathbf{I} - \mathbf{K}_k \mathbf{H}_k) \mathbf{P}_{k-1} (\mathbf{I} - \mathbf{K}_k \mathbf{H}_k)^T + \mathbf{K}_k \mathbf{R}_k \mathbf{K}_k^T. \quad (3.25)$$

Finally, before initializing the algorithm, it is necessary to provide an initial estimate of \mathbf{x} and of the \mathbf{P} matrix, as well as defining the values for the measurement covariance matrix \mathbf{R}_k . In this case, the latter matrix will be viewed as constant since it is assumed that the covariance of the measurements does not change in time. This is a somewhat coarse approximation since it has been established by the algebraic solution simulations of Chapter 2.5 that the measurement errors grow with distance.

The following step is to define how the available measurements will be related to the problem constants and create an observation model to be implemented in (3.15)

3.2 Loosely Coupled Implementation

A first approach to the problem of defining a measurement model is to use the results from the algebraic solution as measurements, which are the measured positions of the target and are directly related to the problem constants by (3.1). With this observation model, there is a further degree of freedom in the choice of assumed value of the constant acceleration, \mathbf{a}_0 , which can be assumed to be zero, for a constant velocity motion approximation, or any value as the most general case. Both cases will be evaluated and thus for the time of the k^{th} measurement, at time t_k , the zero acceleration case transforms (3.1) into

$$\mathbf{p}_t(t_k) = \mathbf{p}_{t_0} + \mathbf{v}_{t_0} t_k, \quad (3.26)$$

and the problem reduces to the determination of only two constants. Making the measurement

$$\mathbf{y}_k = \mathbf{p}_m(t)(t_k) = \begin{bmatrix} p_{mx}(t_k) & p_{my}(t_k) & p_{mz}(t_k) \end{bmatrix}^T \quad (3.27)$$

and the parameter vector

$$\mathbf{x} = \begin{bmatrix} \mathbf{p}_{t_0} & \mathbf{v}_{t_0} \end{bmatrix}^T = \begin{bmatrix} p_{t_0x} & p_{t_0y} & p_{t_0z} & v_{t_0x} & v_{t_0y} & v_{t_0z} \end{bmatrix}^T, \quad (3.28)$$

the matrix \mathbf{H}_k that satisfies (3.4) is

$$\mathbf{H}_k = \begin{bmatrix} \mathbf{I}_3 & t_k \mathbf{I}_3 \end{bmatrix}. \quad (3.29)$$

This solution will be referred to as the Constant Velocity Recursive Least Squares (RLS-V).

For the constant, non-zero acceleration case (3.1) maintains the presented form and the measurements remain given by (3.27). As for the parameter vector, it is given by

$$\begin{aligned} \mathbf{x} &= \begin{bmatrix} \mathbf{p}_{t_0} & \mathbf{v}_{t_0} & \mathbf{a}_{t_0} \end{bmatrix}^T \\ &= \begin{bmatrix} p_{t_0x} & p_{t_0y} & p_{t_0z} & v_{t_0x} & v_{t_0y} & v_{t_0z} & a_{t_0x} & a_{t_0y} & a_{t_0z} \end{bmatrix}^T \end{aligned} \quad (3.30)$$

and the matrix \mathbf{H}_k to satisfy (3.4) now becomes

$$\mathbf{H}_k = \begin{bmatrix} \mathbf{I}_3 & t_k \mathbf{I}_3 & \frac{1}{2} t_k^2 \mathbf{I}_3 \end{bmatrix}. \quad (3.31)$$

This solution will be referred to as the Constant Acceleration Recursive Least Squares (RLS-A).

3.3 Simulation Results

Before applying the developed estimators to the simulation scenarios defined in chapter 2.4, the initial estimates for the parameter vector \mathbf{x} and the estimation-error covariance matrix \mathbf{P} must be chosen and subsequently refined, while the measurement-error covariance matrix must be defined. Since \mathbf{P} can be viewed as a measurement of the confidence in the result of the estimation, this value must be larger initially, the lower the confidence in the initial estimate. For all the simulated trajectories, the initial estimate for the parameter vector is chosen as

$$\hat{\mathbf{x}}_0^{RLS-V} = \mathbf{0}_{6 \times 1} \quad (3.32a)$$

$$\hat{\mathbf{x}}_0^{RLS-A} = \mathbf{0}_{9 \times 1}. \quad (3.32b)$$

The values in (3.32a) and (3.32b) represent an initial complete lack of information regarding the true values of any of the parameters.

For the loosely coupled solutions, as a starting point, the values for the \mathbf{R}_0 and \mathbf{P}_0 matrices were defined as the identity matrix of appropriate size for each algorithm. After extensive simulations, the values for these matrices which lower the total estimate error were found to be

$$\mathbf{R}_0^{RLS-V} = \mathbf{I}_{6 \times 6} \quad (3.33a)$$

$$\mathbf{P}_0^{RLS-V} = 1000 \mathbf{I}_{6 \times 6} \quad (3.33b)$$

$$\mathbf{R}_0^{RLS-A} = \mathbf{I}_{9 \times 9} \quad (3.34a)$$

$$\mathbf{P}_0^{RLS-A} = 1000 \mathbf{I}_{9 \times 9}. \quad (3.34b)$$

Analyzing the values in (3.33) and (3.34), it is possible to match these with their theoretical expected values. The estimate-error covariance matrices are high as expected, representing the uncertainty of the initial estimates, and the measurement-error covariance matrices are the order of magnitude of the measurement errors, as seen in chapter 2.5.

With these values, the resulting estimates produced position errors shown in Fig. 3.1 and 3.2 and characterized in Tables 3.1 and 3.2.

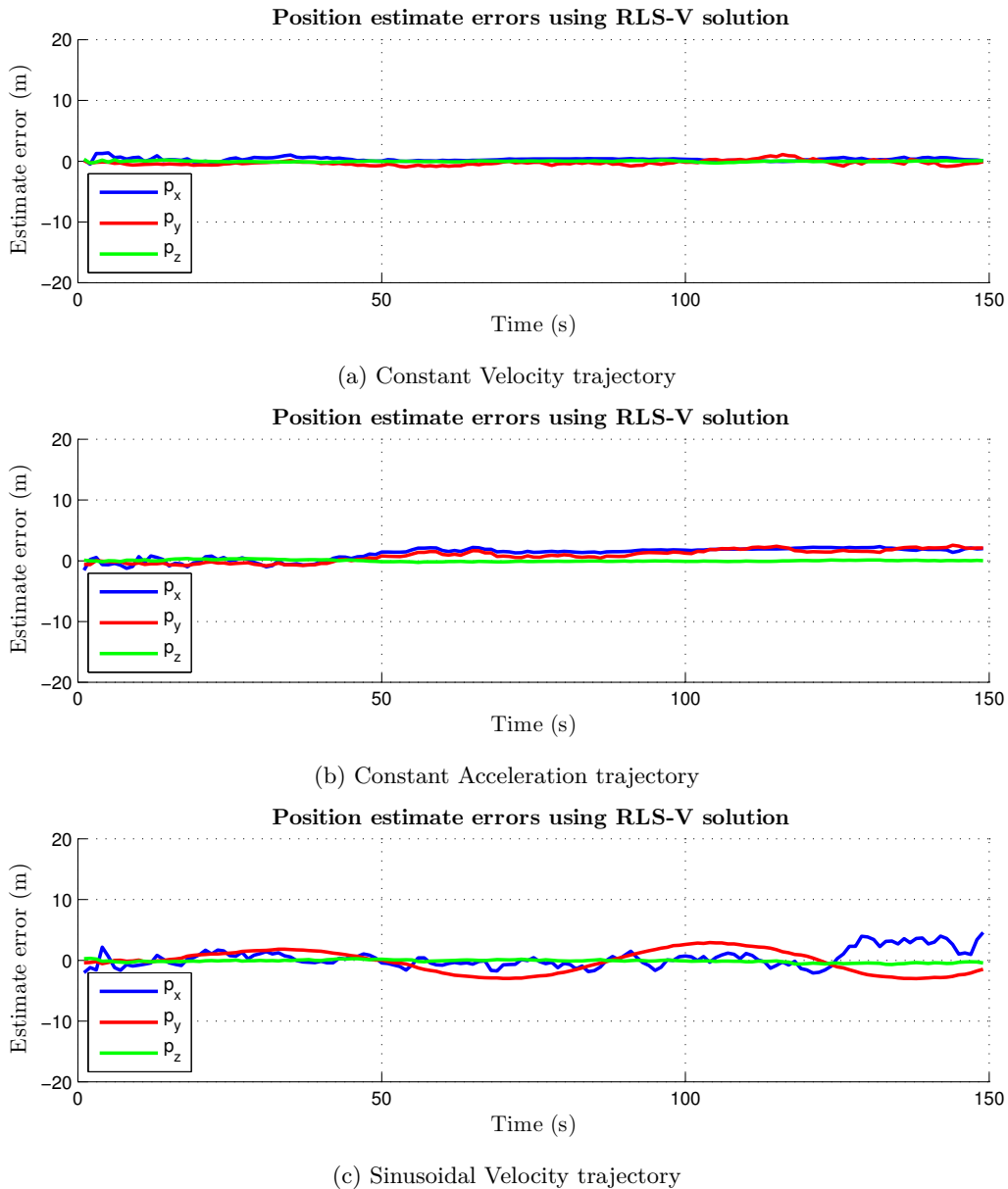


Figure 3.1: Position estimate errors of the RLS-V solution

Finally, the total position errors that can be computed using the norm of the vector difference between the estimate and the true position. These values can be seen in Fig. 3.3, 3.4, and 3.5. In order to compare the solutions, the Root Mean Square (RMS) estimate error is computed for the final 50 seconds of simulation and presented in Table 3.3.

	$p_x (m)$		$p_y (m)$		$p_z (m)$	
	μ	σ	μ	σ	μ	σ
Constant Velocity	0.4379	0.6915	-0.4537	0.3619	-0.0120	0.0874
Constant Acceleration	1.1265	0.9811	0.7005	0.8963	-0.0093	0.0878
Sinusoidal Velocity	0.1313	1.6545	-0.2431	1.8068	0.0101	0.1689

Table 3.1: Estimate error mean and standard deviations for RLS-V solution

	$p_x (m)$		$p_y (m)$		$p_z (m)$	
	μ	σ	μ	σ	μ	σ
Constant Velocity	0.4752	0.6682	-0.4715	0.5114	-0.0205	0.1156
Constant Acceleration	0.1919	0.9192	-0.1365	0.5966	-0.0108	0.1209
Sinusoidal Velocity	0.3969	2.0877	-0.2914	1.3272	-0.0077	0.2378

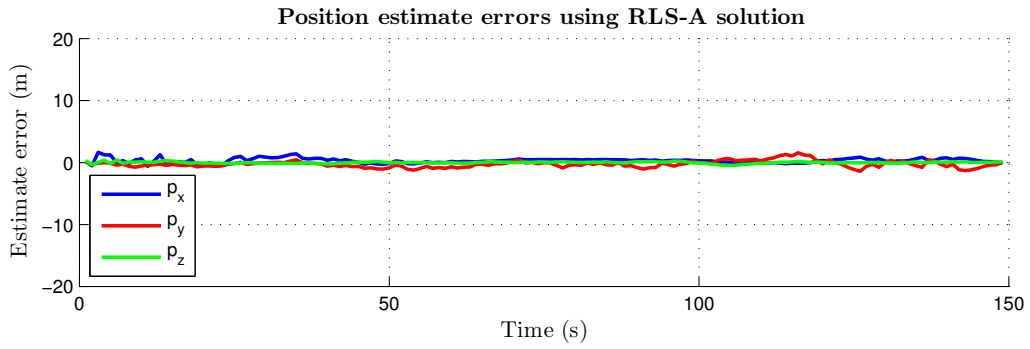
Table 3.2: Estimate error mean and standard deviations for RLS-A solution

From an analysis of the results, a conclusion may be reached that for the cases where the assumptions for the development of the estimators are fulfilled, the estimation errors of these cases are the smallest. Furthermore, it is apparent that when the estimated conditions respect both estimators conditions, the constant velocity (and consequently constant acceleration) their performance is fairly equal. However, for the case in which the conditions only respect the assumptions of the RLS-A, this option maintains the level of performance of the former solutions while the RLS-V loses accuracy the more it progresses in time. Finally, for the sinusoidal velocity case, which does not fully respect the assumptions of either estimator, the performance of both solutions is inferior to the previous situations where the simulated behaviors respected the models predictions.

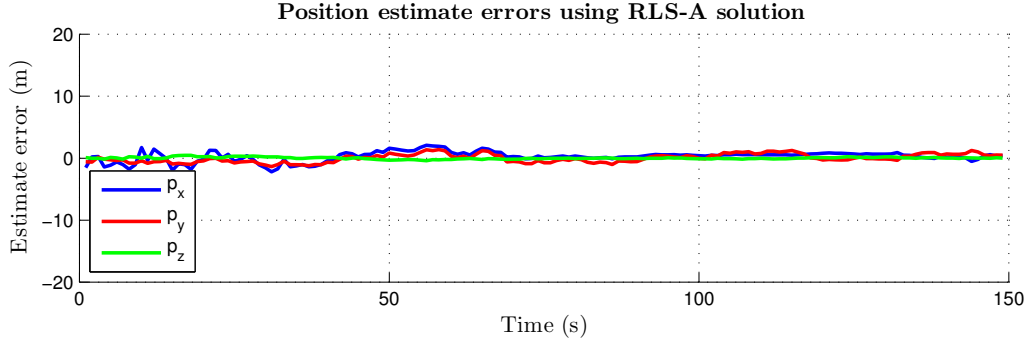
These simulations validate the proposed estimators and through the analysis of the estimation RMS errors in Table 3.3 there is a basis for comparison with future solutions, as well as an idea of the performance level and adequacy of such a solution in the event of a practical application, or implementation in a deployed system.

Simulation	RLS-V	RLS-A	Law of Sines
Constant Velocity	0.6022 (m)	0.8459 (m)	3.0873 (m)
Constant Acceleration	2.6982 (m)	0.8314 (m)	1.6665 (m)
Sinusoidal Velocity	3.1984 (m)	3.3307 (m)	7.8186 (m)

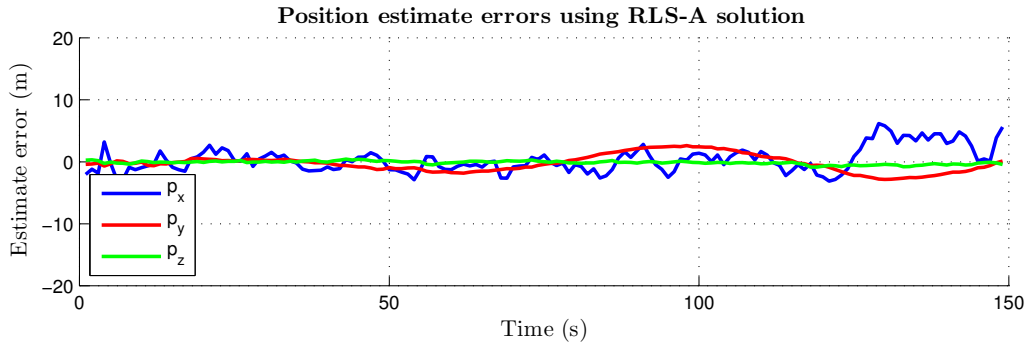
Table 3.3: Estimate RMS error comparisons for the RLS solutions



(a) Constant Velocity trajectory



(b) Constant Acceleration trajectory



(c) Sinusoidal Velocity trajectory

Figure 3.2: Position estimate errors of the RLS-A solution

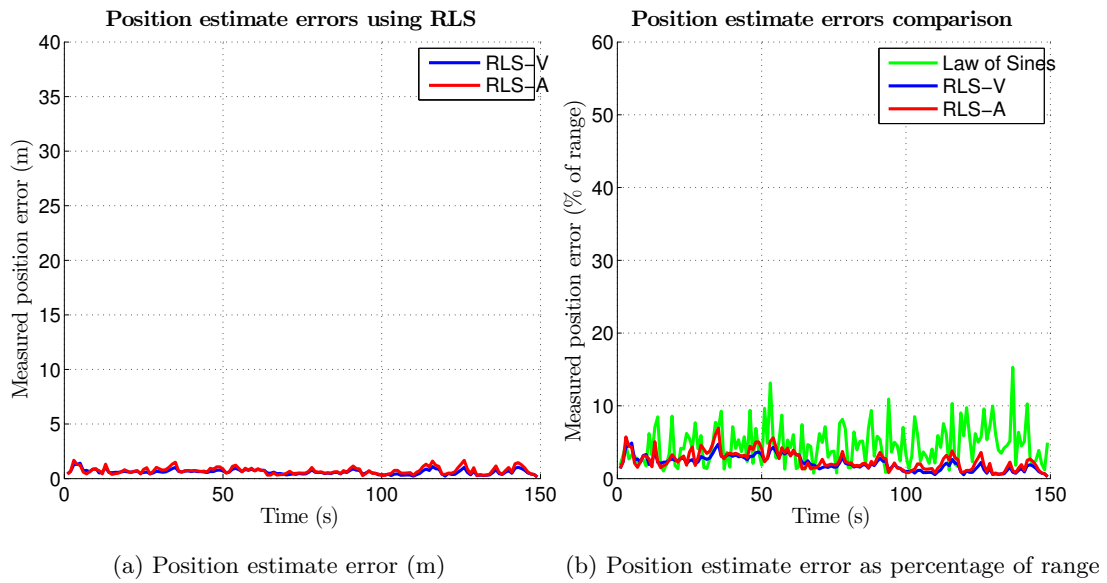


Figure 3.3: Position estimate errors of the RLS estimators for the constant velocity case

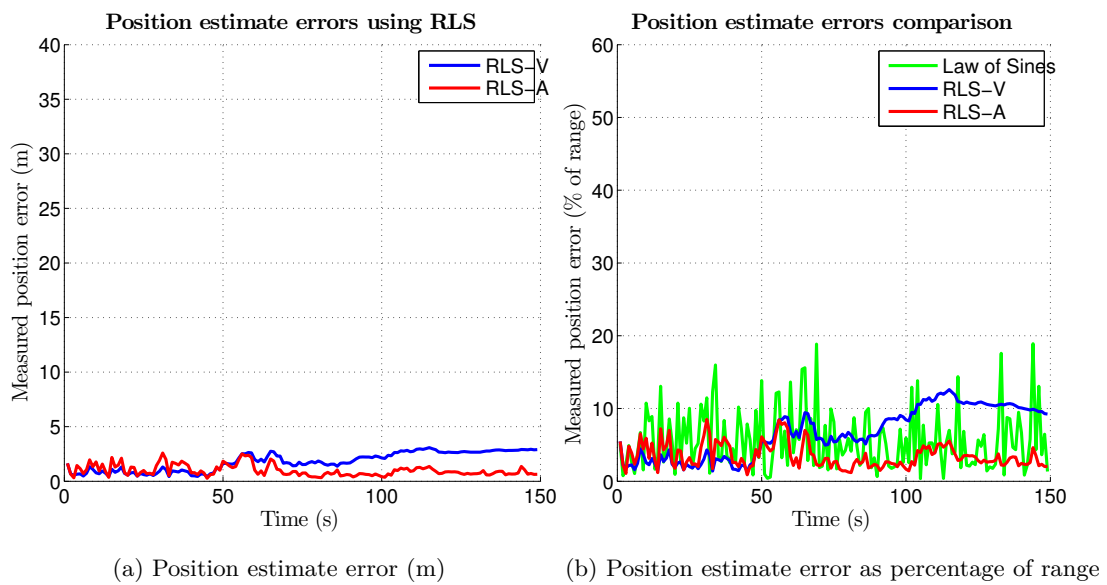
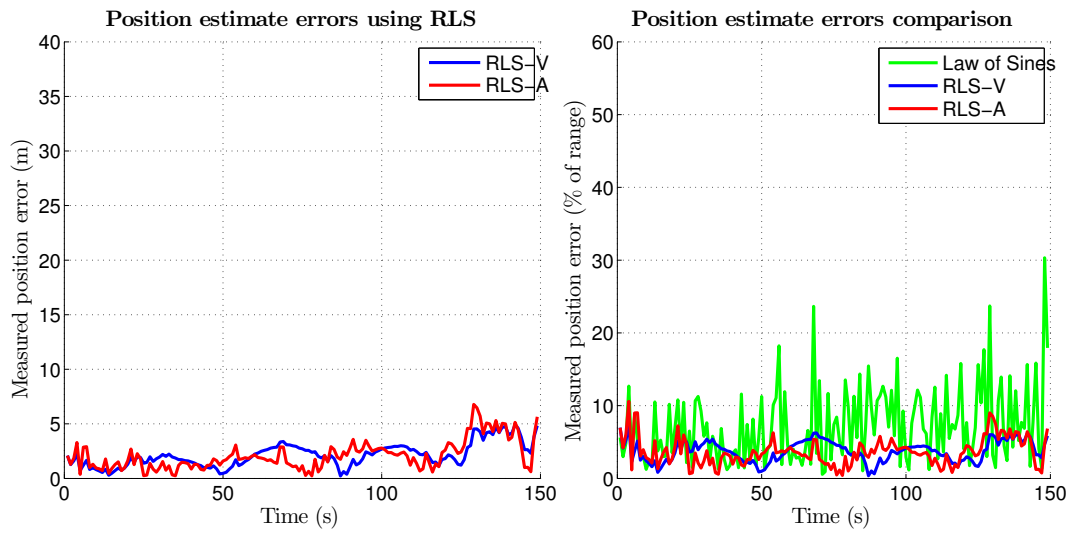


Figure 3.4: Position estimate errors of the RLS estimators for the constant acceleration case



(a) Position estimate error (m)

(b) Position estimate error as percentage of range

Figure 3.5: Position estimate errors of the RLS estimators for the sinusoidal velocity case

Chapter 4

Kalman Filtering

Following the success in the design and simulation of the RLS algorithm, it is desirable to produce an alternative solution that better copes with the situations in which the previous models have difficulties, namely the situation of variable acceleration, and thus a Kalman filter based approach was developed.

4.1 Model Dynamics

Given a problem presented in the state-space form, a Kalman filter allows the estimation of the system states based on direct or indirect measurements of such states, fitted to some assumed model for the system dynamics.

Let (4.1) represent any generic dynamic system in continuous time

$$\dot{\mathbf{x}}(t) = \mathbf{A}(t)\mathbf{x}(t) + \mathbf{B}(t)\mathbf{u}(t) + w(t) \quad (4.1)$$

where $\mathbf{x}(t)$ is the system state, $\mathbf{u}(t)$ is the system input and $w(t)$ is a continuous-time white noise process. Assuming it is possible to direct or indirectly observe the system state, these observations are related to the state by (4.2)

$$\mathbf{y}(t) = \mathbf{C}(t)\mathbf{x}(t) + v(t) , \quad (4.2)$$

where $\mathbf{y}(t)$ is the observation vector, $v(t)$ is a continuous-time noise process and $\mathbf{C}(t)$ is the matrix that obtains the observations from the states.

In the present problem, tracking a moving target involves the estimation of its position and velocity. Additionally, the estimation of its acceleration may be advantageous to reduce errors in the velocity estimate. Firstly, only the position and velocity of the target are estimated, this gives the problem state

$$\mathbf{x}(t)^{K-V} = \left[\mathbf{p}_t(t)^T \quad \mathbf{v}_t(t)^T \right]^T . \quad (4.3)$$

Let

$$\dot{\mathbf{p}}_t(t) = \mathbf{v}_t(t) \quad (4.4)$$

and

$$\dot{\mathbf{v}}_t(t) = \mathbf{a}_t(t) . \quad (4.5)$$

Then,

$$\begin{aligned} \dot{\mathbf{x}}(t)^{K-V} &= \begin{bmatrix} \dot{\mathbf{p}}_t(t)^T & \dot{\mathbf{v}}_t(t)^T \end{bmatrix}^T \\ &= \begin{bmatrix} \mathbf{v}_t(t)^T & \mathbf{a}_t(t)^T \end{bmatrix}^T , \end{aligned} \quad (4.6)$$

and the matrix that satisfies (4.1) is

$$\mathbf{A}(t)^{K-V} = \begin{bmatrix} \mathbf{0}_{3 \times 3} & \mathbf{I}_3 \\ \mathbf{0}_{3 \times 3} & \mathbf{0}_{3 \times 3} \end{bmatrix} . \quad (4.7)$$

Since, by definition of the problem, the input, $\mathbf{u}(t)$, in the dynamic equation of the target is unknown, it is assumed non-existent, $\mathbf{B}(t)\mathbf{u}(t)$ disappears, and the dynamic equation is fully defined. The row of zeros in the $\mathbf{A}(t)$ matrix appears because $\mathbf{a}_t(t)$ is not a part of the states considered above and thus the dynamic equation evaluates $\dot{\mathbf{v}}_t(t)$ as zero which corresponds to the modeled assumption of an unvarying velocity. This solution will be referred to as the Velocity Estimating Kalman Filter (Kalman-V).

However, the constant velocity assumption may not be a good enough approximation to the reality. Thus, in order to remove this modeled constraint from the dynamic equation, the addition of the target acceleration in the problem states is considered, resulting in

$$\mathbf{x}(t)^{K-A} = \begin{bmatrix} \mathbf{p}_t(t)^T & \mathbf{v}_t(t)^T & \mathbf{a}_t(t)^T \end{bmatrix}^T . \quad (4.8)$$

Take once again (4.4) and (4.5), and now let

$$\begin{aligned} \dot{\mathbf{x}}(t)^{K-A} &= \begin{bmatrix} \dot{\mathbf{p}}_t(t)^T & \dot{\mathbf{v}}_t(t)^T & \dot{\mathbf{a}}_t(t)^T \end{bmatrix}^T \\ &= \begin{bmatrix} \mathbf{v}_t(t)^T & \mathbf{a}_t(t)^T & \dot{\mathbf{a}}_t(t)^T \end{bmatrix}^T , \end{aligned} \quad (4.9)$$

the matrix that satisfies (4.1) is now

$$\mathbf{A}(t)^{K-A} = \begin{bmatrix} \mathbf{0}_{3 \times 3} & \mathbf{I}_3 & \mathbf{0}_{3 \times 3} \\ \mathbf{0}_{3 \times 3} & \mathbf{0}_{3 \times 3} & \mathbf{I}_3 \\ \mathbf{0}_{3 \times 3} & \mathbf{0}_{3 \times 3} & \mathbf{0}_{3 \times 3} \end{bmatrix} . \quad (4.10)$$

There is still a row of zeros in the $\mathbf{A}(t)$ matrix, now representing a lack of model for the variation of acceleration based on the estimated states. This solution evaluates $\dot{\mathbf{a}}_t(t)$ as zero which is somewhat analogous to modeling a constant acceleration and will be henceforth referred to as the Accelleration Estimating Kalman Filter (Kalman-A).

Finally, the available measurements must be related to the problem states in order to complete the $\mathbf{C}_t(t)$ matrix of (4.2). Two different methods of defining this measurement matrix, their advantages and shortcomings will be the subject of sections 4.3 and 4.4. However, prior to the investigation of these solutions, some alterations to the way the state-space system is treated will be considered.

4.2 Kalman Filtering Theory

At this point in the work, the models and dynamics are considered in continuous time. Although this is the most realistic representation of the system, the computations of all the subsequent algorithms are usually implemented in digital computers, using discrete time. A very detailed description of the continuous time Kalman filter derivation and algorithm is present in [14]. For the remainder of this work, the discrete time Kalman filter will be used.

In order to use the discrete time Kalman filter, the problem must now be presented in a discrete state space form. Let k represent any discrete time moment, and let \mathbf{x}_k be the problem state at that moment. Any discrete-time system may be represented as

$$\mathbf{x}_k = f_{k-1}(\mathbf{x}_{k-1}, \mathbf{u}_{k-1}, w_{k-1}) \quad (4.11a)$$

$$\mathbf{y}_k = h_{k-1}(\mathbf{x}_k, v_k) , \quad (4.11b)$$

which in the case of a linear system simplifies as

$$\mathbf{x}_k = \mathbf{F}_{k-1}\mathbf{x}_{k-1} + \mathbf{G}_{k-1}\mathbf{u}_{k-1} + w_{k-1} \quad (4.12a)$$

$$\mathbf{y}_k = \mathbf{H}_k\mathbf{x}_k + v_k , \quad (4.12b)$$

where \mathbf{F}_{k-1} is the state transition matrix for the previous state, \mathbf{H}_k is the observation model matrix, \mathbf{y}_k is the measurement vector, \mathbf{u}_{k-1} is the input in the previous moment, \mathbf{G}_{k-1} is the matrix that describes the effect of the previous moment inputs on the state, and w_{k-1} and v_k are Additive White Gaussian Noise (AWGN) processes with covariance matrices defined respectively as \mathbf{Q}_k and \mathbf{R}_k . The same reasoning applies to the \mathbf{G}_{k-1} matrix and \mathbf{u}_{k-1} vector as for the continuous time $\mathbf{B}(t)$ and $\mathbf{u}(t)$ elements, respectively, and accordingly will be assumed zero and omitted.

In order to present the current system in discrete-time form, the \mathbf{A} and \mathbf{C} matrices of the continuous model must be discretized into the \mathbf{F}_{k-1} and \mathbf{H}_k matrices respectively. Resorting to the Step Invariant method, for the \mathbf{A} matrix this is done through the matrix exponential, shown in (4.13), where Δt is the time difference between steps $k - 1$ and k . Applying (4.13) to (4.7) and (4.10), results in (4.14) and (4.15), which are the discrete-time state transition matrices for the Kalman-V and Kalman-A approaches respectively. In the case of the \mathbf{C} matrix, no discretization is required since the measurement model does not represent a dynamic relation but rather a relation between the state and the measurements, and thus is the same in discrete or continuous-time, simply changing denomination to \mathbf{H}_k .

$$\mathbf{F}_{k-1} = e^{\mathbf{A}\Delta t} \quad (4.13)$$

$$\mathbf{F}_{k-1}^{K-V} = \begin{bmatrix} \mathbf{I}_3 & \Delta t\mathbf{I}_3 \\ \mathbf{0}_{3 \times 3} & \mathbf{I}_3 \end{bmatrix} \quad (4.14)$$

$$\mathbf{F}_{k-1}^{K-A} = \begin{bmatrix} \mathbf{I}_3 & \Delta t \mathbf{I}_3 & \frac{1}{2} \Delta t^2 \mathbf{I}_3 \\ \mathbf{0}_{3 \times 3} & \mathbf{I}_3 & \Delta t \mathbf{I}_3 \\ \mathbf{0}_{3 \times 3} & \mathbf{0}_{3 \times 3} & \mathbf{I}_3 \end{bmatrix} \quad (4.15)$$

Even though a measurement model has yet to be defined, the Kalman filter algorithm may be derived and shown.

The Kalman filter [6] estimates the state at any given moment based on the previous state and any available measurements. The way through which this is accomplished is by first estimating the current state based on the state propagation from the best estimate for the previous state and subsequently correcting that estimate with the aid of the available measurements. Let us define $\hat{\mathbf{x}}_k^-$ as the result of the estimation based on the propagation of the previous state and $\hat{\mathbf{x}}_k^+$ as the state estimate after the measurement correction. These shall be referred to as the *a priori* and *a posteriori* estimates.

Assuming that, after each step, the best estimate of the state is the *a posteriori* estimate, the *a priori* estimate at step k is computed similarly to (4.12a). For the present conditions we then have

$$\hat{\mathbf{x}}_k^- = \mathbf{F}_{k-1} \hat{\mathbf{x}}_{k-1}^+ . \quad (4.16)$$

Since all estimates are implicitly corrupted with the process noise w_{k-1} and the measurement noise v_k , an estimate of the error level of the current estimate must be computed. This is taken into account by maintaining an estimate of an estimate-error covariance matrix, \mathbf{P}_k . Because the state estimate is corrupted by noise in two different operations, the \mathbf{P}_k matrix estimate must be updated according to each of the operations. For the *a priori* state estimation operation, an *a priori* covariance matrix estimate is defined as the covariance of the *a priori* estimate error

$$\mathbf{P}_k^- = E \left[(\mathbf{x}_k - \hat{\mathbf{x}}_k^-)^T (\mathbf{x}_k - \hat{\mathbf{x}}_k^-) \right] , \quad (4.17)$$

and substituting (4.12a) into (4.17), assuming uncorrelated noise and expanding gives

$$\mathbf{P}_k^- = \mathbf{F}_{k-1} \mathbf{P}_{k-1}^+ \mathbf{F}_{k-1}^T + \mathbf{Q}_{k-1} . \quad (4.18)$$

With the state propagation estimate obtained, the interest now lies in correcting this estimate with the information provided by the measurement. Recovering the measurement update equation for the Recursive Least Squares (RLS) estimator (3.16), considering now that the estimate being computed is $\hat{\mathbf{x}}_k^+$ instead of $\hat{\mathbf{x}}_k$ and the previous estimate is given by $\hat{\mathbf{x}}_k^-$ instead of $\hat{\mathbf{x}}_{k-1}$, it can be rewritten as

$$\hat{\mathbf{x}}_k^+ = \hat{\mathbf{x}}_k^- + \mathbf{K}_k (\mathbf{y}_k - \mathbf{H}_k \hat{\mathbf{x}}_k^-) , \quad (4.19)$$

with \mathbf{K}_k , now denominated the Kalman Gain, given by (3.24) substituting the previous step estimation-error covariance matrix \mathbf{P}_{k-1}^+ with the most recent estimate for the covariance matrix, \mathbf{P}_k^- , resulting in

$$\mathbf{K}_k = \mathbf{P}_k^- \mathbf{H}_k^T (\mathbf{H}_k \mathbf{P}_k^- \mathbf{H}_k^T + \mathbf{R}_k)^{-1} . \quad (4.20)$$

Finally, the estimation-error covariance matrix must again be updated to reflect the added information. The new estimate is denominated the *a posteriori* estimation-error covariance matrix and is given by

$$\mathbf{P}_k^+ = (\mathbf{I} - \mathbf{K}_k \mathbf{H}_k) \mathbf{P}_k^- (\mathbf{I} - \mathbf{K}_k \mathbf{H}_k)^T + \mathbf{K}_k \mathbf{R}_k \mathbf{K}_k^T, \quad (4.21)$$

which is almost identical to (3.25) but with the previous estimation-error covariance matrix given by \mathbf{P}_k^- instead of \mathbf{P}_{k-1} .

With all the matrices defined, the Kalman Filter algorithm may be applied starting with the time update of the state estimate (4.16) and the estimation-error covariance (4.18), followed by the computation of the Kalman gain (4.20), the measurement update of the state estimate (4.19), and estimation-error covariance matrix (4.18).

Finally, the only remaining step required is to define the measurement model matrix \mathbf{H}_k , the initial state estimate $\hat{\mathbf{x}}_0^+$, initial estimation-error covariance matrix \mathbf{P}_0 , and the measurement noise covariance \mathbf{R} and model noise covariance \mathbf{Q} matrices. During the simulation phase, the initial estimates and noise matrices were given initial plausible values which were refined through repeated simulation runs.

4.3 Loosely Coupled Solution

As previously accomplished in the RLS estimator, a loosely coupled solution will be developed using the position results from the algebraic solution. Accordingly, the measurements for this approach will be the position results of the algebraic solution, $\tilde{\mathbf{p}}_t(t)$. Defining the measurement

$$\mathbf{y}(t) = \mathbf{p}_{mt}(t) \quad (4.22)$$

with

$$\mathbf{p}_{mt}(t) = \mathbf{p}_t(t) + v, \quad (4.23)$$

then for the Kalman-V case results in the measurement model matrix

$$\mathbf{C}_{K-V} = \begin{bmatrix} \mathbf{I}_3 & \mathbf{0}_{3 \times 3} \end{bmatrix} \quad (4.24)$$

or, for the Kalman-A case

$$\mathbf{C}_{K-A} = \begin{bmatrix} \mathbf{I}_3 & \mathbf{0}_{3 \times 3} & \mathbf{0}_{3 \times 3} \end{bmatrix}. \quad (4.25)$$

With the measurement model completely defined in continuous-time, in discrete-time the matrix changes denomination but maintains its contents. These discrete-time measurement models are then

$$\mathbf{H}_k^{K-V} = \begin{bmatrix} \mathbf{I}_3 & \mathbf{0}_{3 \times 3} \end{bmatrix} \quad (4.26)$$

for the Kalman-V method, and for the Kalman-A

$$\mathbf{H}_k^{K-A} = \begin{bmatrix} \mathbf{I}_3 & \mathbf{0}_{3 \times 3} & \mathbf{0}_{3 \times 3} \end{bmatrix}. \quad (4.27)$$

The Kalman Filter algorithm has now all of its elements available to implement in simulation.

4.4 Tightly Coupled Solution

After the development of the loosely coupled solution, it is desirable to pursue a filter that would extract as much information from the measurements as possible while at the same time removing the need for external computations. For these reasons, a tightly coupled Kalman filter was designed in order to extract the state information directly from the sensor measurements.

Firstly, the system states must be chosen and the system model described. For the following designs, the model assumptions remain the same as those in the previous Kalman filters namely the creation of two distinct filters, the velocity estimating filter, the Velocity estimating EKF (EKF-V), and the acceleration estimating filter, the Acceleration estimating EKF (EKF-A). As a starting point, the states and state propagation are assumed the same as in the previous filters, and any available sensor measurements will be expressed as functions of the state variables.

The available measurements are the elements \mathbf{d}_{p_t} , \mathbf{d}_{p_b} , $\mathbf{d}_{p_{tb}}$, and $\|\mathbf{p}_b\|$ from Fig. 2.1. Still from the figure, remembering that \mathbf{d}_{p_t} is the direction cosine of the target position, \mathbf{p}_t , let it be described as

$$\mathbf{d}_{p_t} = \frac{\mathbf{p}_t}{\|\mathbf{p}_t\|} . \quad (4.28)$$

Analogously, for the transponder position, \mathbf{p}_b , and the target position in relation to the transponder, \mathbf{p}_{tb} , let their direction cosines, \mathbf{d}_{p_b} and $\mathbf{d}_{p_{tb}}$ respectively, be expressed as

$$\mathbf{d}_{p_b} = \frac{\mathbf{p}_b}{\|\mathbf{p}_b\|} \quad (4.29)$$

and

$$\mathbf{d}_{p_{tb}} = \frac{\mathbf{p}_{tb}}{\|\mathbf{p}_{tb}\|} . \quad (4.30)$$

Finally, the direction cosine $\mathbf{d}_{p_{tb}}$ may be expressed as a function of \mathbf{p}_t and \mathbf{p}_b . Attending to Fig. 2.1, and since the \mathbf{p}_t , \mathbf{p}_b and \mathbf{p}_{tb} vectors form a closed path, \mathbf{p}_{tb} can be expressed as the vector difference (4.31)

$$\mathbf{p}_{tb} = \mathbf{p}_t - \mathbf{p}_b . \quad (4.31)$$

Expressing the \mathbf{p}_{tb} vector as the product between its length and direction cosine in (4.31) results in

$$\|\mathbf{p}_{tb}\|\mathbf{d}_{p_{tb}} = \mathbf{p}_t - \mathbf{p}_b . \quad (4.32)$$

Using (4.31) and (4.32), $\mathbf{d}_{p_{tb}}$ can be defined as

$$\mathbf{d}_{p_{tb}} = \frac{\mathbf{p}_t - \mathbf{p}_b}{\|\mathbf{p}_t - \mathbf{p}_b\|} , \quad (4.33)$$

With the four sensor measurements now expressed as function of the state, the measurement vector \mathbf{y}_k is built from (4.28), (4.29) and (4.33) as

$$\mathbf{y}_k = \left[\mathbf{d}_{p_t} \quad \mathbf{d}_{p_b} \quad \mathbf{d}_{p_{tb}} \quad \|\mathbf{p}_b\| \right]^T = \left[\frac{\mathbf{p}_t}{\|\mathbf{p}_t\|}^T \quad \frac{\mathbf{p}_b}{\|\mathbf{p}_b\|}^T \quad \frac{\mathbf{p}_t - \mathbf{p}_b}{\|\mathbf{p}_t - \mathbf{p}_b\|}^T \quad \|\mathbf{p}_b\| \right]^T \quad (4.34)$$

This measurement vector is only related to the target position state with the necessity to have the calculation of the transponder position. In order to circumvent this, and to add a degree of precision to the estimates, the state shall be augmented with the transponder's position and velocity for the EKF-V, and the transponder's position, velocity and acceleration for the EKF-A.

Furthermore, the measurement vector is time-varying and not a linear combination of the states, thus the filter cannot be a linear Kalman filter. A simple way of overcoming this problem is to transform the filter into an extended Kalman filter. The principle of the Extended Kalman Filter (EKF) is to linearize the non-linear system around the *a posteriori* estimate at the previous time step before applying the state-update step and around the *a priori* estimate at the present time step before the measurement-update step of the regular Kalman filter. Here is presented the series of steps required to produce the filter.

Firstly, the system must be presented as the common system and measurement equations as follows. For the present case, the known inputs are considered non-existent as previously justified and thus, shall be omitted. Taking (4.12a) and (4.12b), linearizing \mathbf{x}_k around the *a posteriori* estimate $\mathbf{x}_{k-1} = \hat{\mathbf{x}}_{k-1}^+$ gives

$$\mathbf{x}_k = \mathbf{F}_{k-1}\mathbf{x}_{k-1} + \mathbf{L}_{k-1}w_{k-1} , \quad (4.35)$$

with

$$\mathbf{F}_{k-1} = \left. \frac{\partial f_{k-1}}{\partial \mathbf{x}} \right|_{\hat{\mathbf{x}}_{k-1}^+} \quad (4.36a)$$

$$\mathbf{L}_{k-1} = \left. \frac{\partial f_{k-1}}{\partial \mathbf{w}} \right|_{\hat{\mathbf{x}}_{k-1}^+} , \quad (4.36b)$$

and expanding \mathbf{y}_k around the *a priori* estimate $\mathbf{x}_k = \hat{\mathbf{x}}_k^-$ gives

$$\mathbf{y}_k = \mathbf{H}_k\mathbf{x}_k + \mathbf{M}_k v_k , \quad (4.37)$$

with

$$\mathbf{H}_k = \left. \frac{\partial h_k}{\partial \mathbf{x}} \right|_{\hat{\mathbf{x}}_k^-} \quad (4.38a)$$

$$\mathbf{M}_k = \left. \frac{\partial h_k}{\partial \mathbf{v}} \right|_{\hat{\mathbf{x}}_k^-} . \quad (4.38b)$$

It is assumed that both noise processes are additive in their respective equations and thus the \mathbf{L}_{k-1} and \mathbf{M}_k matrices are appropriately sized identities. This means that

the regular linear Kalman filter equations may be applied as they were presented. Since the state-space system is already linear, the \mathbf{F}_{k-1} matrix remains as in (4.15) and the time update equations (4.16) and (4.18) may be applied. To obtain the time-variant \mathbf{H}_k matrix from the non-linear measurement, the Jacobian is applied to (4.34) and results in, for the EKF-V

$$\mathbf{H}_k^{E-V} = \frac{d\mathbf{y}_k}{d\mathbf{x}} = \begin{bmatrix} H_{11} & H_{12} & H_{13} & 0 & 0 & 0 & 0 & 0 & 0 & 0 & 0 & 0 & 0 & 0 & 0 \\ H_{21} & H_{22} & H_{23} & 0 & 0 & 0 & 0 & 0 & 0 & 0 & 0 & 0 & 0 & 0 & 0 \\ H_{31} & H_{32} & H_{33} & 0 & 0 & 0 & 0 & 0 & 0 & 0 & 0 & 0 & 0 & 0 & 0 \\ 0 & 0 & 0 & 0 & 0 & 0 & H_{47} & H_{48} & H_{49} & 0 & 0 & 0 & 0 & 0 & 0 \\ 0 & 0 & 0 & 0 & 0 & 0 & H_{57} & H_{58} & H_{59} & 0 & 0 & 0 & 0 & 0 & 0 \\ 0 & 0 & 0 & 0 & 0 & 0 & H_{67} & H_{68} & H_{69} & 0 & 0 & 0 & 0 & 0 & 0 \\ H_{71} & H_{72} & H_{73} & 0 & 0 & 0 & H_{77} & H_{78} & H_{79} & 0 & 0 & 0 & 0 & 0 & 0 \\ H_{81} & H_{82} & H_{83} & 0 & 0 & 0 & H_{87} & H_{88} & H_{89} & 0 & 0 & 0 & 0 & 0 & 0 \\ H_{91} & H_{92} & H_{93} & 0 & 0 & 0 & H_{97} & H_{98} & H_{99} & 0 & 0 & 0 & 0 & 0 & 0 \\ 0 & 0 & 0 & 0 & 0 & 0 & H_{107} & H_{108} & H_{109} & 0 & 0 & 0 & 0 & 0 & 0 \end{bmatrix}, \quad (4.39)$$

and for the EKF-A

$$\mathbf{H}_k^{E-A} = \frac{d\mathbf{y}_k}{d\mathbf{x}} = \begin{bmatrix} H_{11} & H_{12} & H_{13} & 0 & 0 & 0 & 0 & 0 & 0 & 0 & 0 & 0 & 0 & 0 & 0 & 0 & 0 \\ H_{21} & H_{22} & H_{23} & 0 & 0 & 0 & 0 & 0 & 0 & 0 & 0 & 0 & 0 & 0 & 0 & 0 & 0 \\ H_{31} & H_{32} & H_{33} & 0 & 0 & 0 & 0 & 0 & 0 & 0 & 0 & 0 & 0 & 0 & 0 & 0 & 0 \\ 0 & 0 & 0 & 0 & 0 & 0 & 0 & 0 & 0 & H_{47} & H_{48} & H_{49} & 0 & 0 & 0 & 0 & 0 \\ 0 & 0 & 0 & 0 & 0 & 0 & 0 & 0 & 0 & H_{57} & H_{58} & H_{59} & 0 & 0 & 0 & 0 & 0 \\ 0 & 0 & 0 & 0 & 0 & 0 & 0 & 0 & 0 & H_{67} & H_{68} & H_{69} & 0 & 0 & 0 & 0 & 0 \\ H_{71} & H_{72} & H_{73} & 0 & 0 & 0 & 0 & 0 & 0 & H_{77} & H_{78} & H_{79} & 0 & 0 & 0 & 0 & 0 \\ H_{81} & H_{82} & H_{83} & 0 & 0 & 0 & 0 & 0 & 0 & H_{87} & H_{88} & H_{89} & 0 & 0 & 0 & 0 & 0 \\ H_{91} & H_{92} & H_{93} & 0 & 0 & 0 & 0 & 0 & 0 & H_{97} & H_{98} & H_{99} & 0 & 0 & 0 & 0 & 0 \\ 0 & 0 & 0 & 0 & 0 & 0 & 0 & 0 & 0 & H_{107} & H_{108} & H_{109} & 0 & 0 & 0 & 0 & 0 \end{bmatrix}, \quad (4.40)$$

where

$$\begin{aligned}
H_{11} &= \frac{p_{ty}^2 + p_{tz}^2}{\sigma_1} & H_{12} &= \frac{-p_{tx}p_{ty}}{\sigma_1} \\
H_{13} &= \frac{-p_{tx}p_{tz}}{\sigma_1} & H_{21} &= \frac{-p_{tx}p_{ty}}{\sigma_1} \\
H_{22} &= \frac{p_{tx}^2 + p_{tz}^2}{\sigma_1} & H_{23} &= \frac{-p_{ty}p_{tz}}{\sigma_1} \\
H_{31} &= \frac{-p_{tx}p_{tz}}{\sigma_1} & H_{32} &= \frac{-p_{ty}p_{tz}}{\sigma_1} \\
H_{33} &= \frac{p_{tx}^2 + p_{ty}^2}{\sigma_1} & H_{41} &= \frac{p_{by}^2 + p_{bz}^2}{\sigma_2} \\
H_{42} &= \frac{-p_{bx}p_{by}}{\sigma_2} & H_{43} &= \frac{-p_{bx}p_{bz}}{\sigma_2} \\
H_{51} &= \frac{-p_{bx}p_{by}}{\sigma_2} & H_{52} &= \frac{p_{bx}^2 + p_{bz}^2}{\sigma_2} \\
H_{53} &= \frac{-p_{by}p_{bz}}{\sigma_2} & H_{61} &= \frac{-p_{bx}p_{bz}}{\sigma_2} \\
H_{62} &= \frac{-p_{by}p_{bz}}{\sigma_2} & H_{63} &= \frac{p_{bx}^2 + p_{by}^2}{\sigma_2} \\
H_{11} &= \frac{(p_{ty} - p_{by})^2 + (p_{tz} - p_{bz})^2}{\sigma_3} & H_{12} &= \frac{-(p_{tx} - p_{bx})(p_{ty} - p_{by})}{\sigma_3} \\
H_{13} &= \frac{-(p_{tx} - p_{bx})(p_{tz} - p_{bz})}{\sigma_3} & H_{21} &= \frac{-(p_{tx} - p_{bx})(p_{ty} - p_{by})}{\sigma_3} \\
H_{22} &= \frac{(p_{tx} - p_{bx})^2 + (p_{tz} - p_{bz})^2}{\sigma_3} & H_{23} &= \frac{-(p_{ty} - p_{by})(p_{tz} - p_{bz})}{\sigma_3} \\
H_{31} &= \frac{-(p_{tx} - p_{bx})(p_{tz} - p_{bz})}{\sigma_3} & H_{32} &= \frac{-(p_{ty} - p_{by})(p_{tz} - p_{bz})}{\sigma_3} \\
H_{33} &= \frac{(p_{tx} - p_{bx})^2 + (p_{ty} - p_{by})^2}{\sigma_3} & \sigma_1 &= (p_{tx}^2 + p_{ty}^2 + p_{tz}^2)^{\frac{3}{2}} \\
\sigma_2 &= (p_{bx}^2 + p_{by}^2 + p_{bz}^2)^{\frac{3}{2}} & \sigma_3 &= ((p_{tx} - p_{bx})^2 + (p_{ty} - p_{by})^2 + (p_{tz} - p_{bz})^2)^{\frac{3}{2}}
\end{aligned} \tag{4.41}$$

With these results, the measurement-update equations (4.20), (4.19) and (4.21) may be applied as previously described.

4.5 Simulation Results

In order to verify the validity of the filters developed in the current chapter, numerical simulations were performed using the simulation setup previously defined in chapter 2.4. To recap, the simulations comprise a range of artificial trajectories which model some assumed target behaviors. These will be fed to the estimators in order to evaluate the importance of the design considerations in the final performance, as well as compare the designs to each other. Again, the presented results will be the ones obtained after extensive iterative manual tuning of the measurement-error and estimate-error covariance matrices. Additionally, the best results from the present chapter's filters will be compared to the best results from the ones designed in Chapter 3 for trade-off considerations in increased computational and model complexities.

For this set of simulations the initial estimates were assumed totally unknown and the following initial values were given for the Kalman-V and Kalman-A respectively

$$\mathbf{x}_0^{K-V} = \mathbf{0}_{6 \times 1} \tag{4.42a}$$

$$\mathbf{x}_0^{K-A} = \mathbf{0}_{9 \times 1} . \tag{4.42b}$$

As for the \mathbf{R}_0 , \mathbf{P}_0 and \mathbf{Q}_0 matrices, these were firstly defined as unity matrices of

appropriate size and then manually tuned to values that gave the best estimates of position. After extensive testing the best values for these matrices were found to be

$$\mathbf{Q}_0^{K-V} = 5 \times 10^{-4} \mathbf{I}_{6 \times 6} \quad (4.43a)$$

$$\mathbf{R}_0^{K-V} = 5 \mathbf{I}_{3 \times 3} \quad (4.43b)$$

$$\mathbf{P}_0^{K-V} = \begin{bmatrix} 100 \mathbf{I}_{3 \times 3} & \mathbf{0}_{3 \times 3} \\ \mathbf{0}_{3 \times 3} & 100 \mathbf{I}_{3 \times 3} \end{bmatrix} \quad (4.43c)$$

for the Kalman-V filter, and

$$\mathbf{Q}_0^{K-A} = 1 \times 10^{-7} \mathbf{I}_{9 \times 9} \quad (4.44a)$$

$$\mathbf{R}_0^{K-A} = 5 \mathbf{I}_{3 \times 3} \quad (4.44b)$$

$$\mathbf{P}_0^{K-A} = \begin{bmatrix} 100 \mathbf{I}_{3 \times 3} & \mathbf{0}_{3 \times 3} & \mathbf{0}_{3 \times 3} \\ \mathbf{0}_{3 \times 3} & 5 \mathbf{I}_{3 \times 3} & \mathbf{0}_{3 \times 3} \\ \mathbf{0}_{3 \times 3} & \mathbf{0}_{3 \times 3} & \mathbf{I}_{3 \times 3} \end{bmatrix} \quad (4.44c)$$

for the Kalman-A filter.

The results of the simulations performed on the Kalman-V and Kalman-A solutions are presented in Fig. 4.1 and 4.2, with the error characteristics described in Tables 4.1 and 4.2.

	$p_x (m)$		$p_y (m)$		$p_z (m)$	
	μ	σ	μ	σ	μ	σ
Constant Velocity	0.4953	0.8269	-0.4519	0.4350	-0.0165	0.0905
Constant Acceleration	0.7261	0.6421	0.2567	0.5611	-0.0133	0.0902
Sinusoidal Velocity	0.2306	1.8529	-0.1212	1.6718	0.0014	0.1909

Table 4.1: Estimate error mean and standard deviations for Kalman-V solution

	$p_x (m)$		$p_y (m)$		$p_z (m)$	
	μ	σ	μ	σ	μ	σ
Constant Velocity	0.4953	0.7564	-0.4949	0.3751	-0.0269	0.0987
Constant Acceleration	0.0584	0.8827	-0.1482	0.5441	-0.0099	0.1081
Sinusoidal Velocity	0.4388	1.6632	-0.5582	2.3360	-0.0023	0.1941

Table 4.2: Estimate error mean and standard deviations for Kalman-A solution

With this in mind, the same process used previously is applied and the norm of the vector difference between the estimate and the real value is computed and the results of this Loosely Coupled solutions are presented for the three artificial trajectories, in Fig. 4.3, 4.4, and 4.5.

Finally, in order to evaluate the relative performance of the simulated situations, Table 4.3 presents the RMS error of the position estimate for the final 50 seconds of simulation.

Simulation	Kalman-V	Kalman-A	RLS-V	RLS-A
Constant Velocity	0.7687 (m)	0.6300 (m)	0.6022 (m)	0.8459 (m)
Constant Acceleration	1.3873 (m)	0.8118 (m)	2.6982 (m)	0.8314 (m)
Sinusoidal Velocity	3.2238 (m)	3.9639 (m)	3.1984 (m)	3.3307 (m)

Table 4.3: Estimate RMS error comparisons for the Kalman filter solutions

From Fig. 4.3 and Table 4.3, we are able to conclude that both designed filters are equivalent in performance for the constant velocity case, with the Kalman-A filter having a slightly more oscillatory behavior in the initial stage. This is the expected behavior for the considered situation since both models accurately describe the modeled motion. The initial oscillatory behavior of the Kalman-A filtered is explained by the fact that it is attempting to estimate the acceleration of the target without any direct measurement information, contrary to the Kalman-V filter that, correctly for the present situation, assumes zero acceleration.

For the constant acceleration case, in Fig. 4.4 we can observe that while initially both filters have similar error, the Kalman-V's error levels rise steadily while the Kalman-A's remain somewhat constant which is supported by the Table. Again, this goes towards the expected outcome. The Kalman-A filter is a better model for the considered situation and as such has a long term better performance than the Kalman-V. The latter considers an oversimplified model that while in the short term compensates for its own inadequacy, fails in the long term to maintain an estimate as good as the more complex model.

Finally, regarding the sinusoidal velocity simulation, we may observe in Fig. 4.5 that both filters exhibit poorer estimates of the target position. This is an expected behavior since, as observed in the Least Squares (LS) solutions, either model is not an accurate representation of the evaluated motion. However, due to the periodicity of the present case, the errors do not grow unbound and we observe periodic decreases in error in regions where the actual trajectory crosses the estimated trajectory. Furthermore, we see a better long term estimate provided by the Kalman-V filter from Table 4.3, while the initial estimate is better by the Kalman-A filter. The fact that the initial estimate is better provided by the Kalman-A filter is due to the beginning of the motion being similar to a constant acceleration motion, while the better long term estimate by the Kalman-V filter is due to the fact that the latter has a faster response to wide variations than the first.

Following the evaluation of the Kalman filters designed in section 4.3, the same procedure was applied to the EKFs designed in section 4.4. The results of the simulations are presented in Fig. 4.6, 4.7, 4.8, 4.9, and 4.10 and in Tables 4.4, 4.5, and 4.6.

Analyzing Fig. 4.8, we can observe that both designed EKFs have similar convergence and performance for the constant velocity case. This is according to expectations and previous results with linear Kalman filters. We see, however, a slightly minor oscil-

	$p_x (m)$		$p_y (m)$		$p_z (m)$	
	μ	σ	μ	σ	μ	σ
Constant Velocity	0.3372	0.1466	-0.3310	0.1456	-0.0135	0.0676
Constant Acceleration	0.4627	0.2590	0.0258	0.3043	-0.0098	0.0954
Sinusoidal Velocity	-0.4628	0.6836	-0.1140	0.5691	0.0243	0.1282

Table 4.4: Estimate error mean and standard deviations for EKF-V solution

	$p_x (m)$		$p_y (m)$		$p_z (m)$	
	μ	σ	μ	σ	μ	σ
Constant Velocity	0.3333	0.2724	-0.3164	0.2644	-0.0135	0.0979
Constant Acceleration	0.4062	0.3447	-0.0464	0.4129	-0.0032	0.1325
Sinusoidal Velocity	-0.1598	1.2425	-0.0671	0.3330	0.0143	0.2153

Table 4.5: Estimate error mean and standard deviations for EKF-A solution

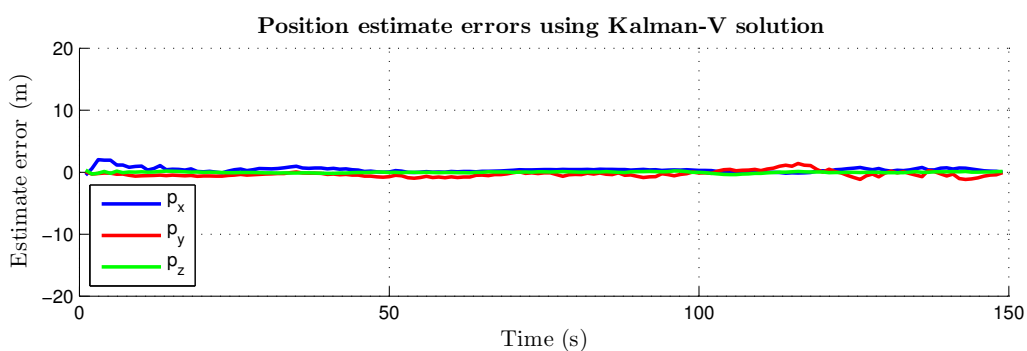
lation of the estimation error of the EKF-V in relation to the EKF-A. This may be the result of the assumed model of the EKF-V being simpler than that of the EKF-A while remaining fully valid for the modeled behavior. In any case, the difference in long term performance while observable from Table 4.6 is negligible for a real world implementation. As far as convergence time is concerned, the EKF-A presents a faster convergence which may be advantageous for certain implementation cases.

Moving on to Fig. 4.9, the results are similar to those observed in the previous simulation. This is surprising since for the same case, using linear Kalman filters produced noticeable differences in long term performance between the two assumed models, namely a continuously growing error in the constant velocity model's estimate. Convergence time and oscillation, however remain sources of performance difference between the models, most importantly the first. By using a motion model in the EKF-V that is less accurate in the simulated situation, we delay convergence even further than for the previous model. The final stretch of simulation, however, presents an almost identical RMS error in the two solutions.

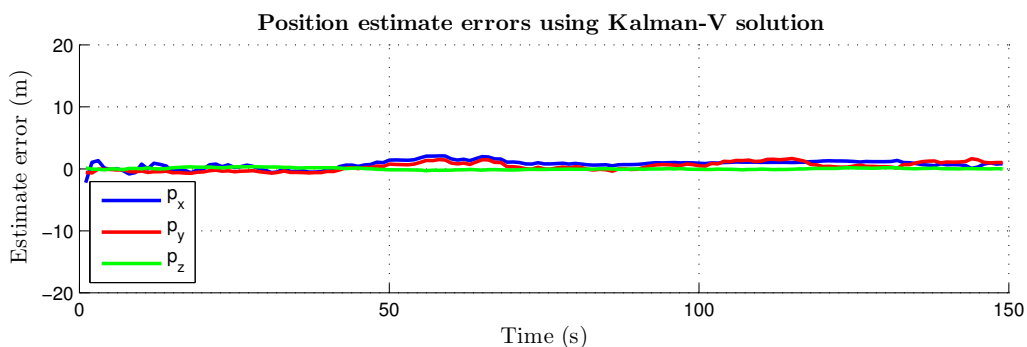
Finally, in Fig. 4.10 both filters present superior performance than in the previous cases with the EKF-V filter having a better and more consistent estimate than the EKF-A. The convergence time is again larger than that of the EKF-A filter.

Simulation	EKF-V	EKF-A	Kalman-V	Kalman-A	RLS-V	RLS-A
Constant Velocity	0.3754 (m)	0.6439 (m)	0.7687 (m)	0.6300 (m)	0.6022 (m)	0.8459 (m)
Constant Acceleration	0.7901 (m)	0.7859 (m)	1.3873 (m)	0.8118 (m)	2.6982 (m)	0.8314 (m)
Sinusoidal Velocity	1.0006 (m)	1.2815 (m)	3.2238 (m)	3.9639 (m)	3.1984 (m)	3.3307 (m)

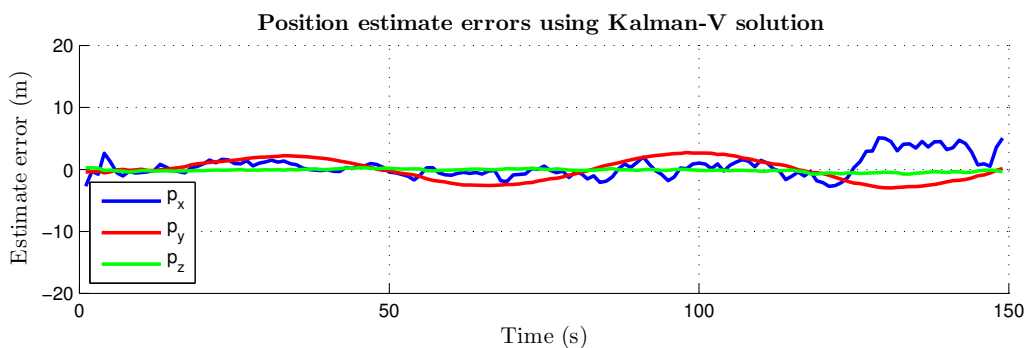
Table 4.6: Estimate RMS error comparisons for the EKF solutions



(a) Constant Velocity trajectory

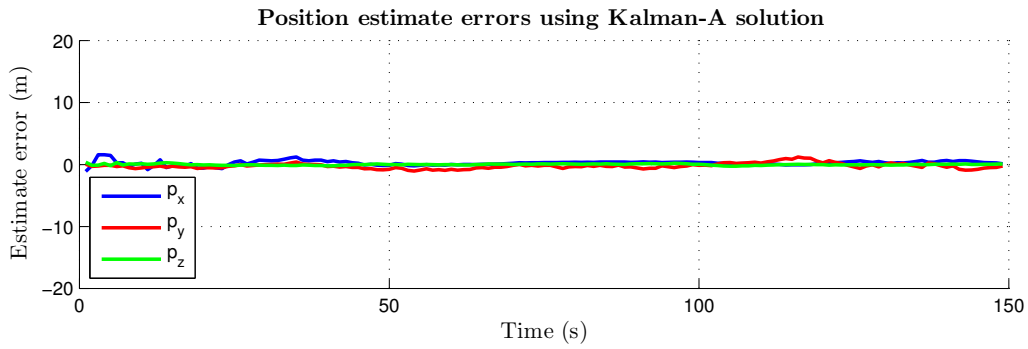


(b) Constant Acceleration trajectory

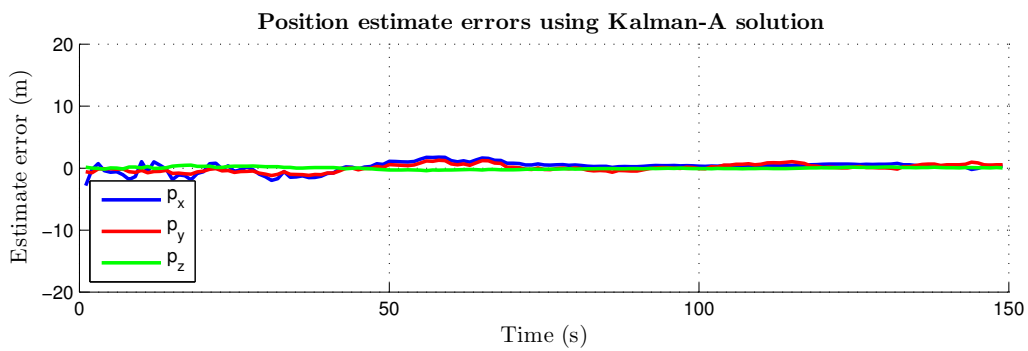


(c) Sinusoidal Velocity trajectory

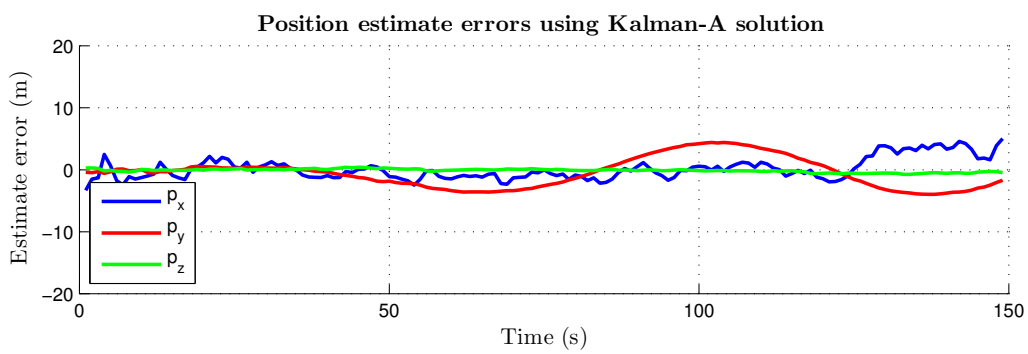
Figure 4.1: Position estimate errors of the Kalman-V solution



(a) Constant Velocity trajectory



(b) Constant Acceleration trajectory



(c) Sinusoidal Velocity trajectory

Figure 4.2: Position estimate errors of the Kalman-A solution

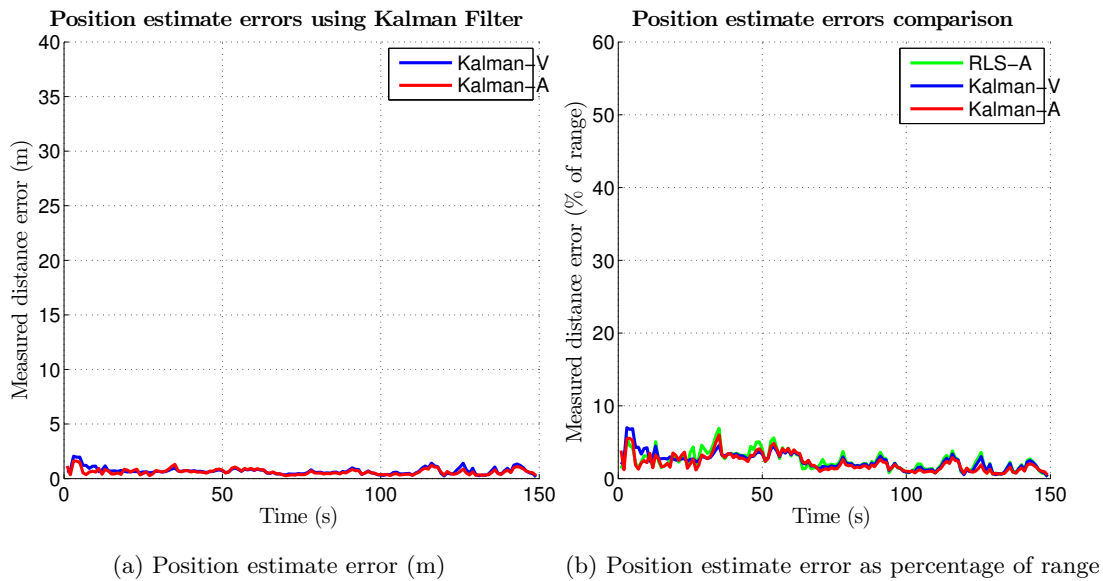


Figure 4.3: Position estimate errors of the Kalman filters for the constant velocity case

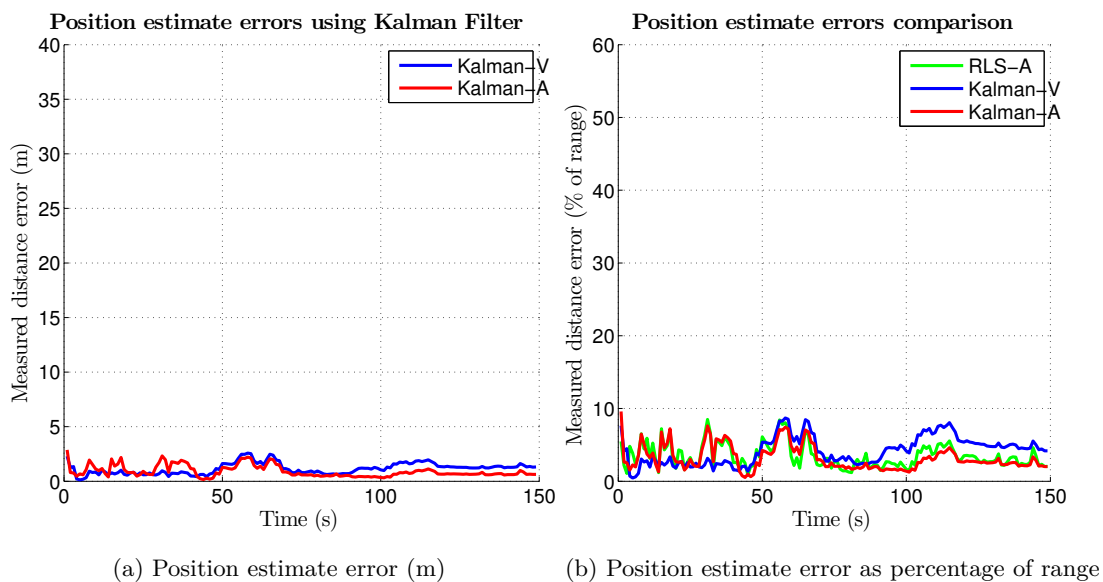
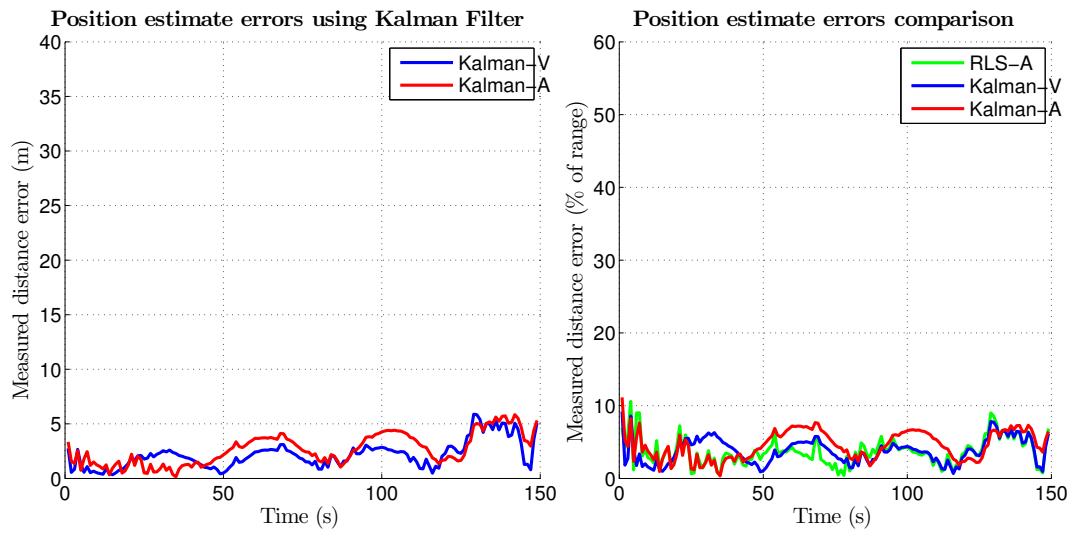


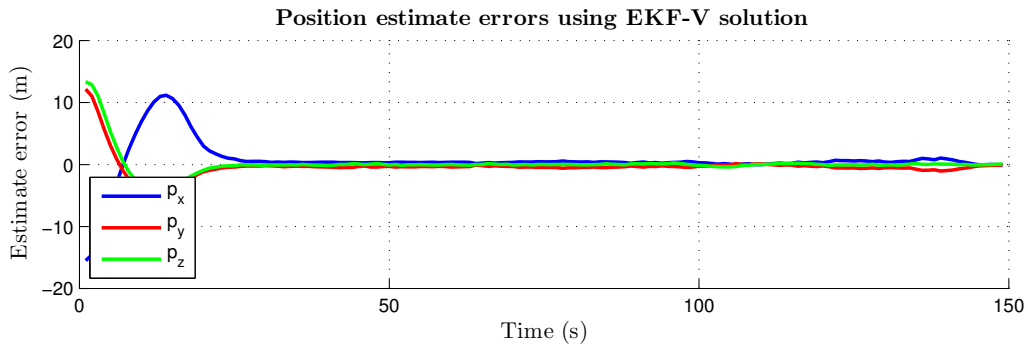
Figure 4.4: Position estimate errors of the Kalman filters for the constant acceleration case



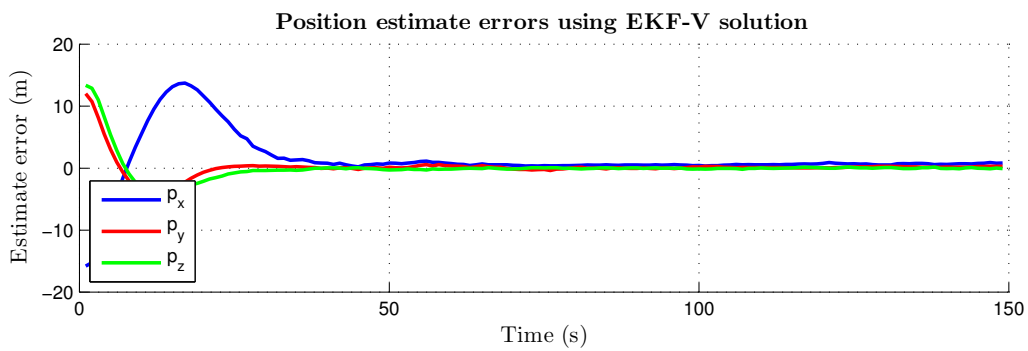
(a) Position estimate error (m)

(b) Position estimate error as percentage of range

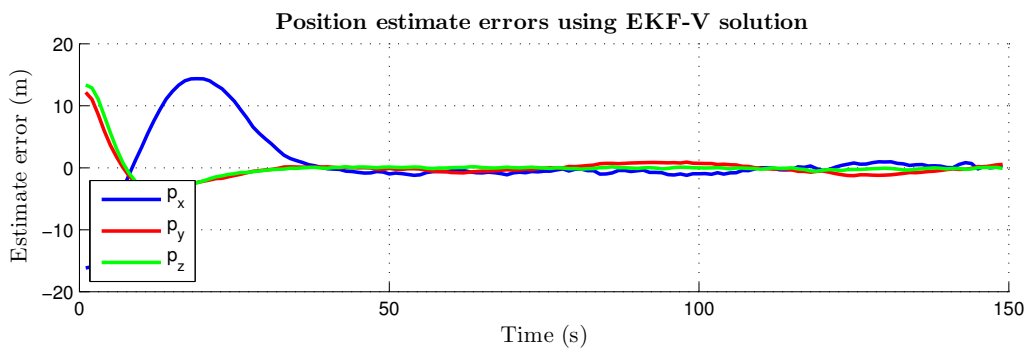
Figure 4.5: Position estimate errors of the Kalman filters for the sinusoidal velocity case



(a) Constant Velocity trajectory

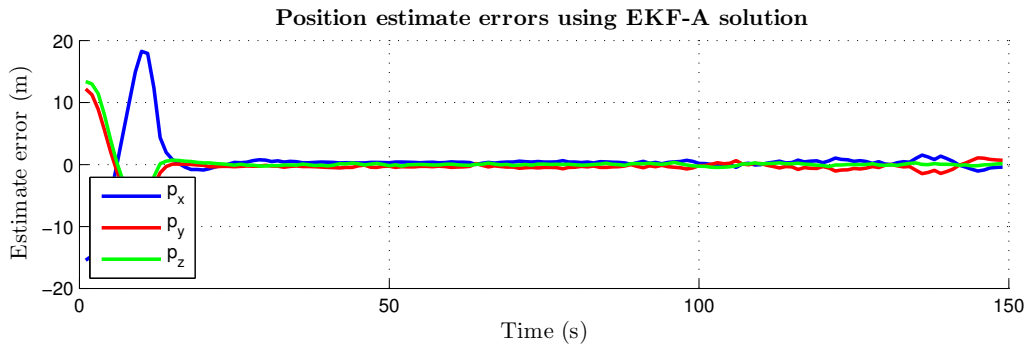


(b) Constant Acceleration trajectory

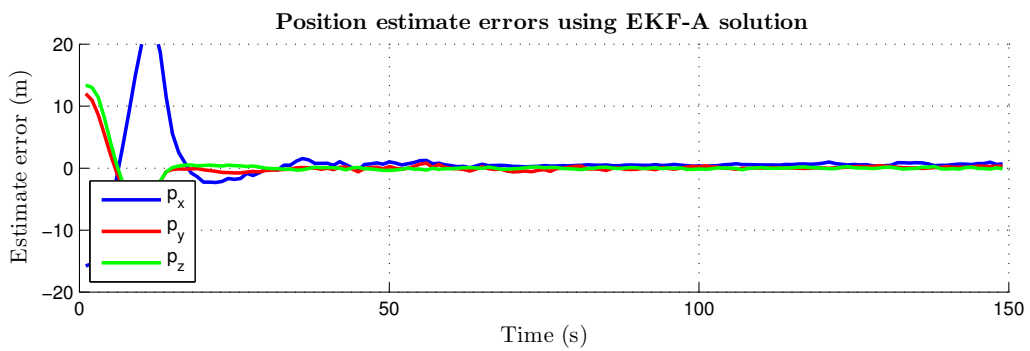


(c) Sinusoidal Velocity trajectory

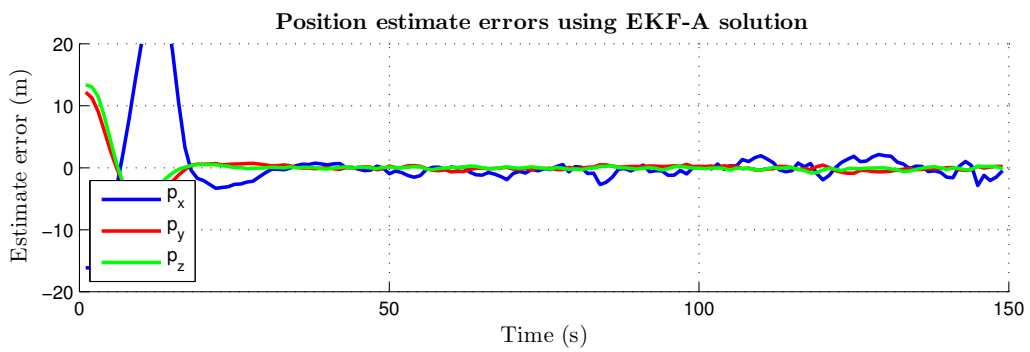
Figure 4.6: Position estimate errors of the EKF-V solution



(a) Constant Velocity trajectory



(b) Constant Acceleration trajectory



(c) Sinusoidal Velocity trajectory

Figure 4.7: Position estimate errors of the EKF-A solution

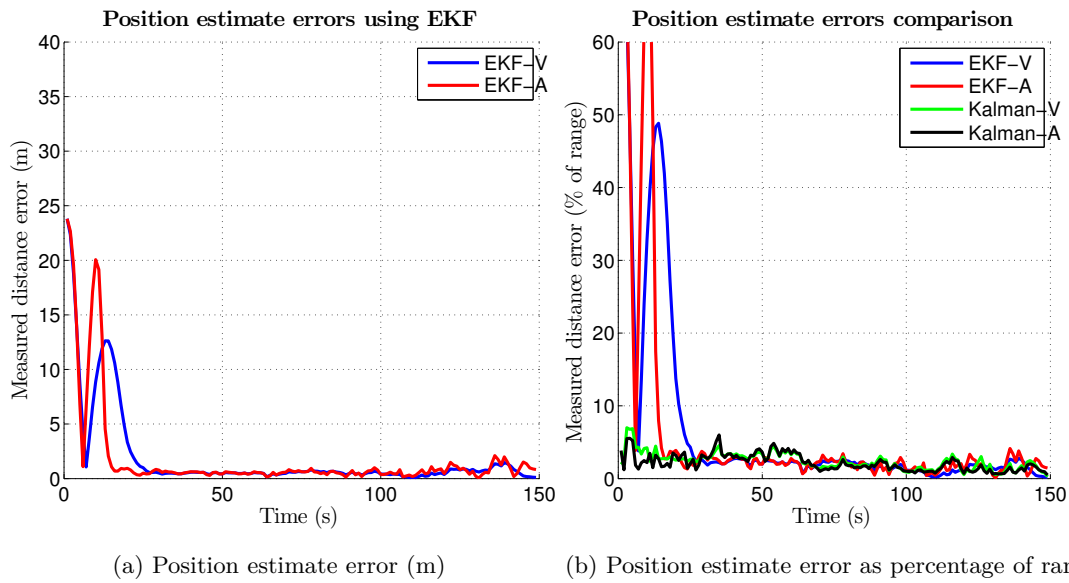


Figure 4.8: Position estimate errors of the Extended Kalman filters for the constant velocity case

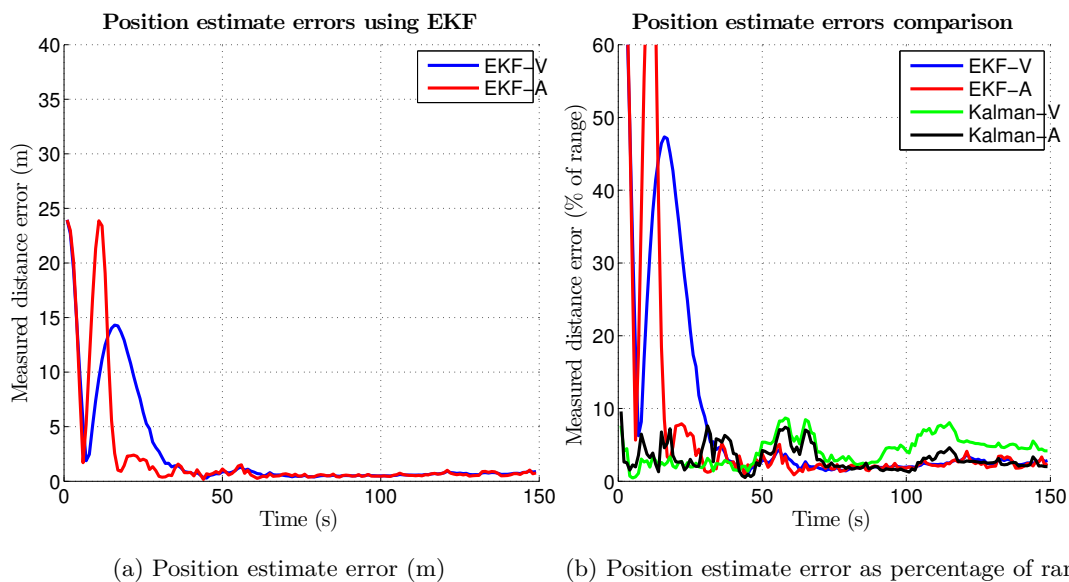


Figure 4.9: Position estimate errors of the Extended Kalman filters for the constant acceleration case

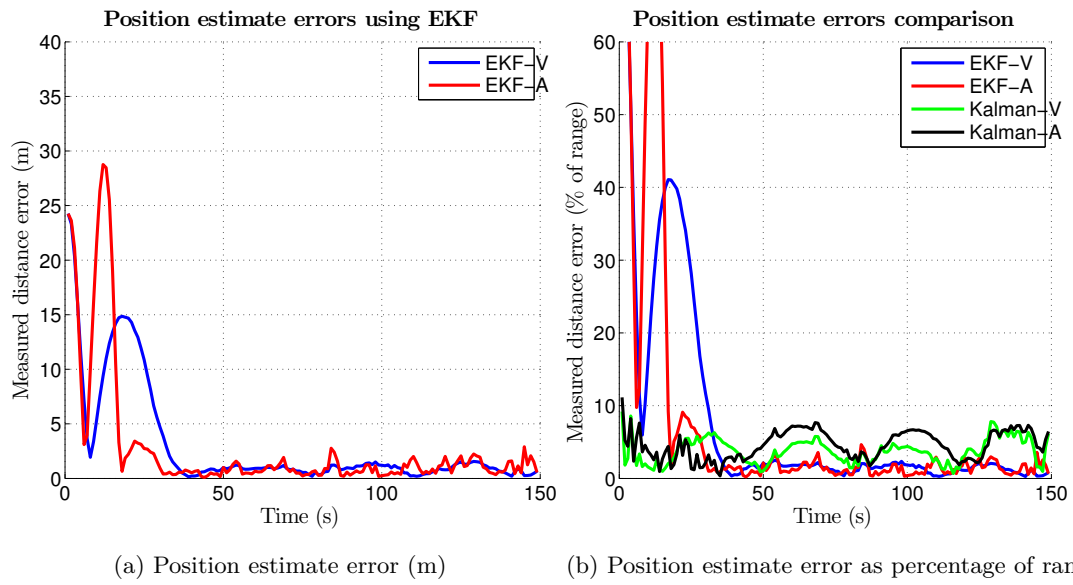


Figure 4.10: Position estimate errors of the Extended Kalman filters for the sinusoidal velocity case

Chapter 5

Conclusion and Future Work

In this work a novel approach to the tracking of underwater moving targets is developed based on acoustic signal Direction of Arrival (DoA) information obtainable with an arrangement of existing Ultra Short Baseline (USBL) array systems and their relative spacial information. The target position is found to be possible to compute with the available measurements and estimation methods are designed that improve the accuracy of the position results and allow for the addition of target velocity and acceleration estimation.

Two algebraic methods are presented that permit the computation of a target position based on the DoA information of an acoustic signal that is emitted by the target, calculated at two different positions where USBL arrays are deployed. Both methods validity conditions were evaluated and described. A set of simulated conditions were formulated to cover a range of possible mission scenarios and were applied to the previously presented methods. It was found possible to calculate a position estimate in all situations, although with varying degrees of error.

LS estimation methods were applied in loosely-coupled linear estimators, for which the measurements were used as the externally computed position values obtained from the algebraic solutions. Two such estimators were designed, one which estimates the target velocity, and one which besides estimating the target velocity, also estimates its acceleration. Due to implementation concerns, LS algorithm was altered in favor of a recursive approach to the estimation into an RLS solution. In this same process, a dependence on the measurement error expected characteristics was added in the form of a measurement-error covariance matrix. The developed methods were simulated in the previously described conditions and the position estimate errors were found to be significantly lower than those of the algebraic solutions.

In order to further improve the quality of the position estimates, Kalman filtering techniques were used. Firstly a loosely-coupled approach was taken which was similar to the RLS solution. The results of the algebraic solutions were used as measurements which gave the system a linear time-invariant observation model. Again, two variants of the filter were presented, both estimating velocity, and one estimating acceleration.

These were also simulated and it was found that either variant presented a comparable or better performance in the constant velocity and constant acceleration simulations than their RLS counterparts, however presenting a worse performance in the sinusoidal velocity case.

Finally, a tightly-coupled approach was taken in order to extract increased accuracy from the measurements and eliminate the need to compute position fixes externally to the estimator. This resulted in a non-linear observation model and the Kalman filter was modified to an Extended Kalman Filter. This solution was derived for both the velocity and the velocity and acceleration estimators and simulated in the same conditions as before. It was found that both models presented better performance than any previous design with the simpler velocity estimating model giving the best estimate in two of the three simulated situations.

With the results obtained in this work, the next step clearly lies in the validation of the premises with field tests, creating a prototype using the already available tools and structures. This path would involve solving certain technical aspects not in the scope of this work such as information transfer between receiver arrays, target signal detection and DoA calculation, and algorithm optimization for a real-time, computationally constrained embedded environment.

Chapter 6

Bibliography

- [1] P. Batista, C. Silvestre, and P. Oliveira. Globally asymptotically stable filters for source localization and navigation aided by direction measurements. In *Decision and Control and European Control Conference (CDC-ECC), 2011 50th IEEE Conference on*, pages 8151–8156, 2011.
- [2] P. Batista, C. Silvestre, and P. Oliveira. On the observability of linear motion quantities in navigation systems. *Systems & Control Letters*, 60(2):101 – 110, 2011.
- [3] P. Batista, C. Silvestre, and P. Oliveira. Globally asymptotically stable filter for navigation aided by direction and depth measurements. In *Decision and Control (CDC), 2012 IEEE 51st Annual Conference on*, pages 6603–6608, 2012.
- [4] Bruno Miguel Simões Carvalho Cardeira. Arquiteturas para navegação inercial/gps com aplicação a veículos autónomos. Master’s thesis, Instituto Superior Técnico, Av. Rovisco Pais, 1, Fevereiro 2009.
- [5] IXSEA. Ixblue gaps brochure. <http://www.ixsea.com/>.
- [6] Rudolph Emil Kalman et al. A new approach to linear filtering and prediction problems. *Journal of basic Engineering*, 82(1):35–45, 1960.
- [7] L. Ljung and T. Söderström. *Theory and practice of recursive identification*. MIT Press series in signal processing, optimization, and control. MIT Press, 1985.
- [8] M. Morgado. *Advanced Ultra-Short Baseline Inertial Navigation Systems*. PhD thesis, Universidade Técnica de Lisboa, Instituto Superior Técnico, Lisboa, 2011.
- [9] M. Morgado, P. Oliveira, and C. Silvestre. Experimental evaluation of a usbl underwater positioning system. In *ELMAR, 2010 PROCEEDINGS*, pages 485–488, 2010.
- [10] M. Morgado, P. Oliveira, C. Silvestre, and J.F. Vasconcelos. Usbl/ins tightly-coupled integration technique for underwater vehicles. In *Information Fusion, 2006 9th International Conference on*, pages 1–8, 2006.

- [11] Census of Marine Life. Scor-tagging document. <http://www.coml.org/>.
- [12] P. Oliveira, C. Silvestre, M. Morgado, K. Erzini, L. Bentes, A. Afonso, F. Hazin, and B. Block. Preliminary results from project mast/am-advanced tracking and telemetry methodologies to study marine animals. In *OCEANS, 2011 IEEE - Spain*, pages 1–6, 2011.
- [13] Wilson J. Rugh. *Linear System Theory*. Prentice Hall, 2nd edition, 1996.
- [14] D. Simon. *Optimal State Estimation: Kalman, H Infinity, and Nonlinear Approaches*. Wiley, 2006.
- [15] VEMCO. V6 coded transmitter (180khz) brochure. <http://www.vemco.com>.
- [16] VEMCO. Vr2w basics manual. <http://www.vemco.com>.